BNL-224218-2023-TECH
EIC-ADD-TN-050

Thermal simulation of the HSR arc BPM Module for EIC

F. Micolon

January 2023

Electron-Ion Collider Project
Brookhaven National Laboratory

U.S. Department of Energy
USDOE Office of Science (SC), Nuclear Physics (NP) (SC-26)

Notice: This technical note has been authored by employees of Brookhaven Science Associates, LLC under Contract No.DE-SC0012704 with the U.S. Department of Energy. The publisher by accepting the technical note for publication acknowledges that the United States Government retains a non-exclusive, paid-up, irrevocable, world-wide license to publish or reproduce the published form of this technical note, or allow others to do so, for United States Government purposes.

DISCLAIMER

This report was prepared as an account of work sponsored by an agency of the United States Government. Neither the United States Government nor any agency thereof, nor any of their employees, nor any of their contractors, subcontractors, or their employees, makes any warranty, express or implied, or assumes any legal liability or responsibility for the accuracy, completeness, or any third party's use or the results of such use of any information, apparatus, product, or process disclosed, or represents that its use would not infringe privately owned rights. Reference herein to any specific commercial product, process, or service by trade name, trademark, manufacturer, or otherwise, does not necessarily constitute or imply its endorsement, recommendation, or favoring by the United States Government or any agency thereof or its contractors or subcontractors. The views and opinions of authors expressed herein do not necessarily state or reflect those of the United States Government or any agency thereof.

Thermal simulation of the HSR arc BPM Module for EIC

F. Micolon, D. Gassner, C. Hetzel, I. Pinayev, K. Matsushima, M. Sangroula, S. Verdu-Andres

Technical Note BNL-224218-2023-TECH / EIC-ADD-TN-050

August 2024

Version	Date	Main modification
0.1	2/1/23	Initial draft
1.0	4/3/2023	First document release.
1.1	10/24/23	New version release – Main changes: - electron cloud heating (section d.5 and e.2) - updated coating thickness for 0.141" cable - updated heat intercept - New appendix VI and VII - Table of content
1.2	8/16/24	New version release – Main changes: - Modification of the welding flange contact condition (Fig. 6) - Button is now copper RRR100 (was RRR10) – minimizes beam RW heating on button (table 2) - Cable outer conductor coating is now RRR10 (was RRR30) - Cable inner conductor is now RRR300 (was RRR100) following recent testing of bulk OFHC copper - Cable coating thickness is now 0.003" for all cables - BPM body is made of stainless steel - more RWH (was copper) - Signal peak voltage reduced - Φ18mm button (was Φ20mm) - References updated

Table of contents

Introduction 2

System integration 2

Model setup 3

Boundary conditions 5

Results and discussion 11

Conclusion 16

Appendix I - Evaluating the loss in a cryogenically cooled RF coaxial cable. 18

Appendix II – Determination of the reference frequency for attenuation 21

Appendix III – Comparison of the coaxial loss model with published data from the LHC 23

Appendix IV – Comparing the simulated attenuation to the manufacturer data 26

Appendix V – Thermal conduction and placement of the heat shield thermalization 29

Appendix VI - Measuring the HSR BPM cable thermal conduction 33

Appendix VII – Heat shield thermal resistance 36

Introduction

The Electron Ion Collider (EIC) Hadron Storage Ring (HSR) will reuse most of the existing superconducting magnets from the RHIC storage ring. However, the existing stripline beam position monitors (BPM) used for RHIC will not be compatible with the planned EIC hadron beam parameters that include higher intensity, shorter bunches, and some operational scenarios with large radial offsets of the beam in the vacuum chamber [1]. To address these challenges, the existing RHIC stripline BPMs will be shielded, and a new BPM design using button pick-ups will be integrated in a new vacuum interconnect/bellows assembly that will be installed adjacent to the existing BPMs.

A thermal analysis of the new arc BPM interconnect housing and button pick-up design has been conducted to assess the effects caused by beam induced resistive wall heating and heating from RF signal propagation through the button pick-up and cables for several operational scenarios. This report will describe the analysis done to quantify the heat transfer and temperature distribution that can be expected on the new HSR cryogenic arc BPM housings, button pick-ups, and cryo-signal cables.

System integration

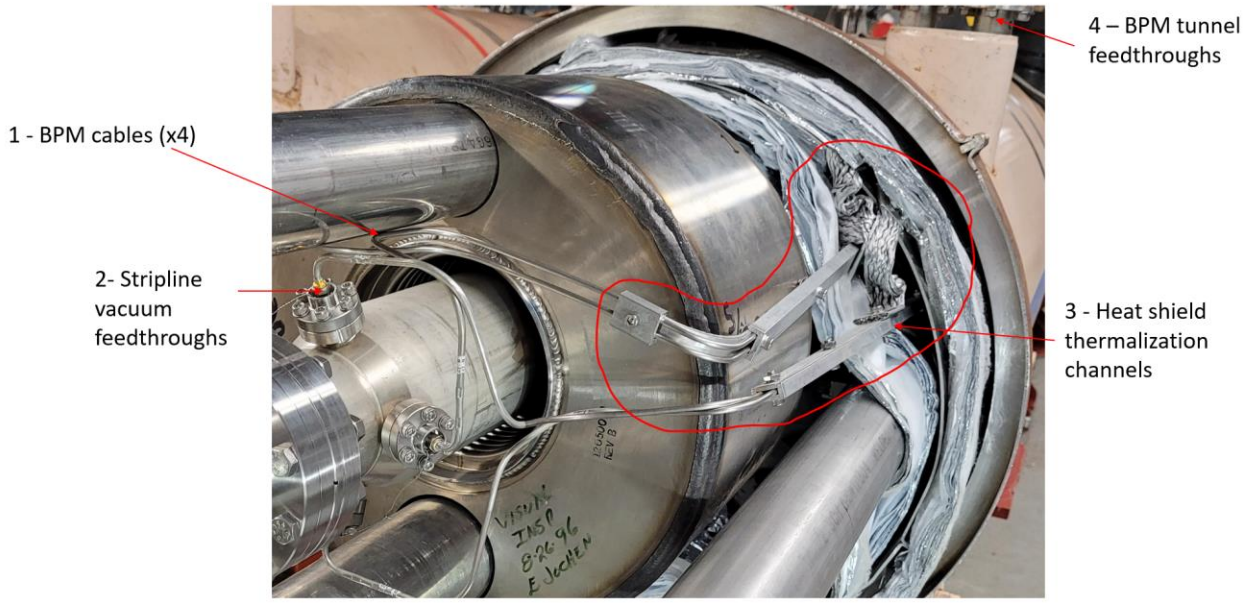


Figure 1 Current BPM cables integration on a RHIC CQS magnet

Fig. 1 shows the current integration of the stripline BPM and their coaxial cables on a RHIC CQS magnet. One end of the cable is connected to the striplines through vacuum feedthroughs (noted 2 on Fig 1). The other end of the cables comes out of the vacuum vessel into the tunnel through vacuum feedthroughs located on the vacuum vessel instrumentation flanges (4 on Fig. 1). In between, the coaxial cables are inserted in aluminum channels that provide heat stationing at the heat shield temperature (3 on Fig. 1). More details are available in Ref. [2].

Since the cables are in vacuum, no convection occurs, and the resistive heat will be conducted away. The current RHIC coaxial cables have a plastic (Tefzel) dielectric, which operate close to their maximum

temperature when RHIC is at the maximum beam intensity. This is due to RF heating and limited operating temperature of the dielectric (see Ref. [3]).

For EIC, the existing stripline BPM will be shielded by the beam screen and new BPMs with button pick-up embedded in the interconnect modules will be installed adjacent (see Fig. 2). We plan to use coaxial signal cables with a SiO2 dielectric which have a much higher operating temperature.

Model setup

1. Geometry and materials

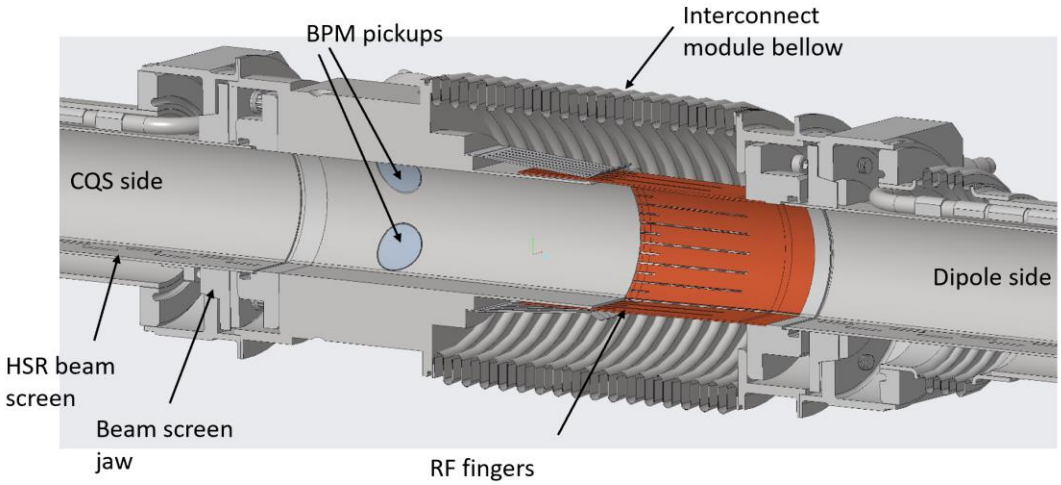


Figure 2 Planned integration of the EIC HSR interconnect module (as of January 2023)

Fig 3. depicts a cross section of the button pick-up BPM implementation and their connectors.

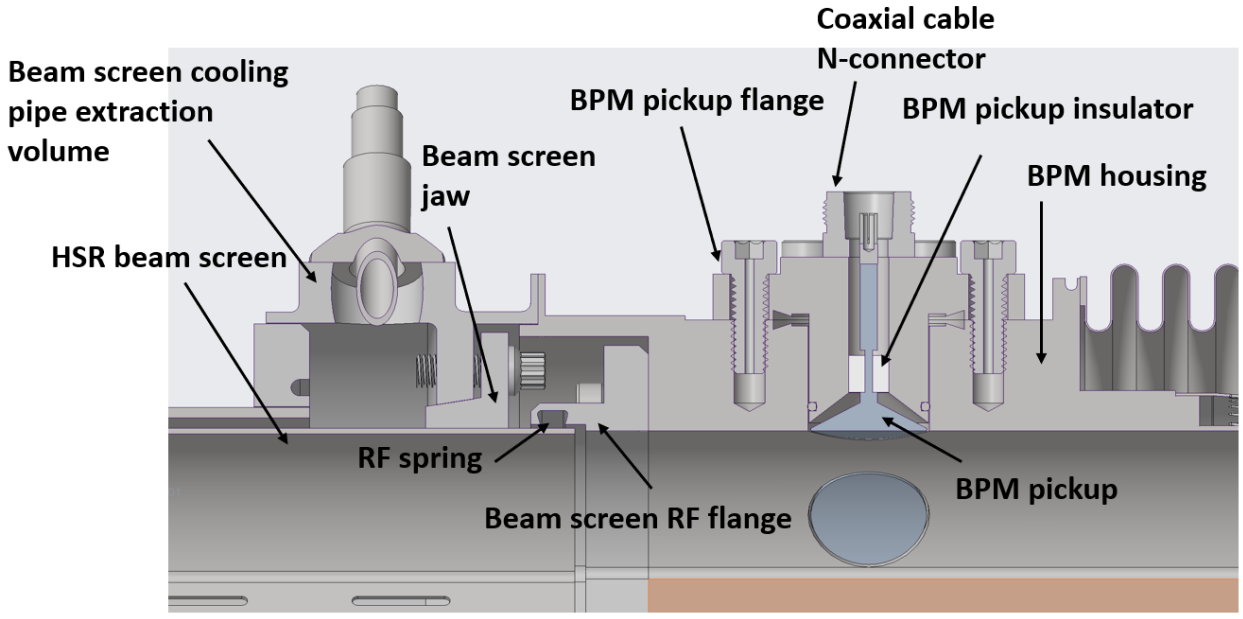


Figure 3 Cross section showing the button BPMs for the EIC HSR (Jan 23)

The finite element (FE) model contains all the BPM housing and components (pickup, insulator, flange) as well as the beam screen cooling pipe extraction module, and jaw assembly (Fig. 4). The beam screen RF flange (Fig. 3) is linked to the beam screen through an RF spring with limited contact. Thus, it is considered that no heat flows through this contact.

The RF fingers included in the interconnect module with the HSR BPM (see Fig.2) are thermally linked to the adjacent magnet, so they are not included in this model and will be treated by a separate analysis (see Ref. [4]).

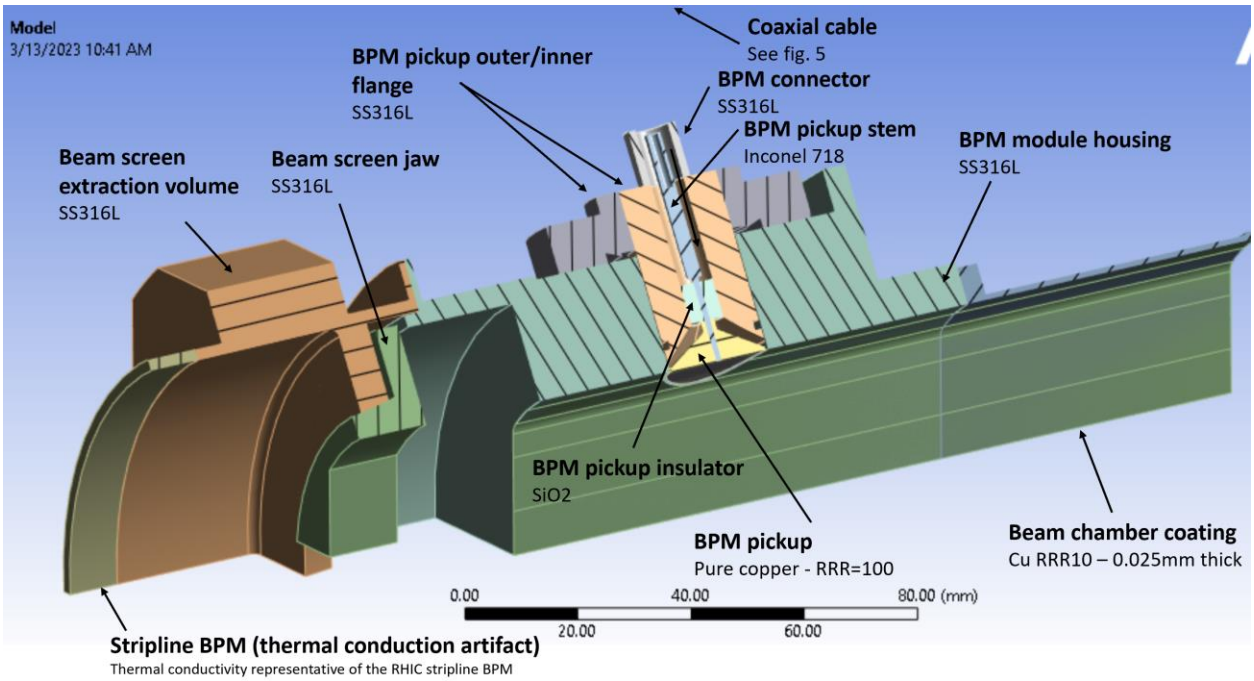


Figure 4 Model 3D geometry representation - 1/8 model

Fig. 5 depicts the coaxial cable cross section modelled. The dimensions retained depend on the specific cable considered and are described in Appendix IV (page 29).

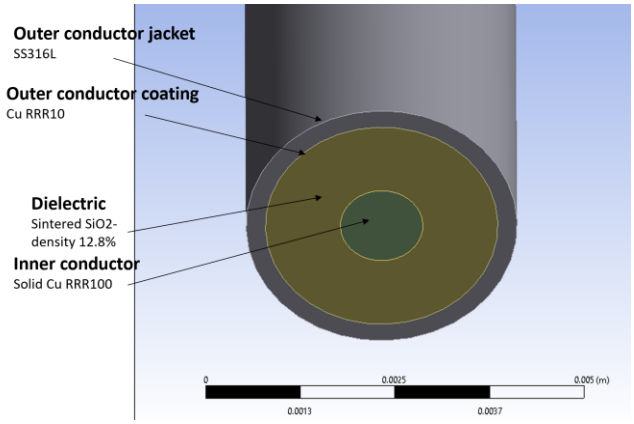


Figure 5 Cross section of the BPM coaxial cable – dimensions used can be found in ***Appendix IV***

2. Contact definition

We have assumed a perfect contact along the radial direction of the coaxial cable between the dielectric material, inner and outer conductors (Fig 5). Fig. 6 represents the contact condition between the other parts of the BPM module model. In addition, the dashed line shows the heat propagation path from the cable to the cold sink (=beam screen).

Following updates from prospective button manufacturer, contacts with limited penetration have been implemented for the button assembly. The pickup/stem contact is laser welded with limited penetration, so it is only considered on the edge. The inner/outer flange are TIG welded on a depth of 0.5 mm (0.02”-0.03” specified by the manufacturer).

Note: A more favorable situation is expected if the button is brazed to the stem instead of tip welded.

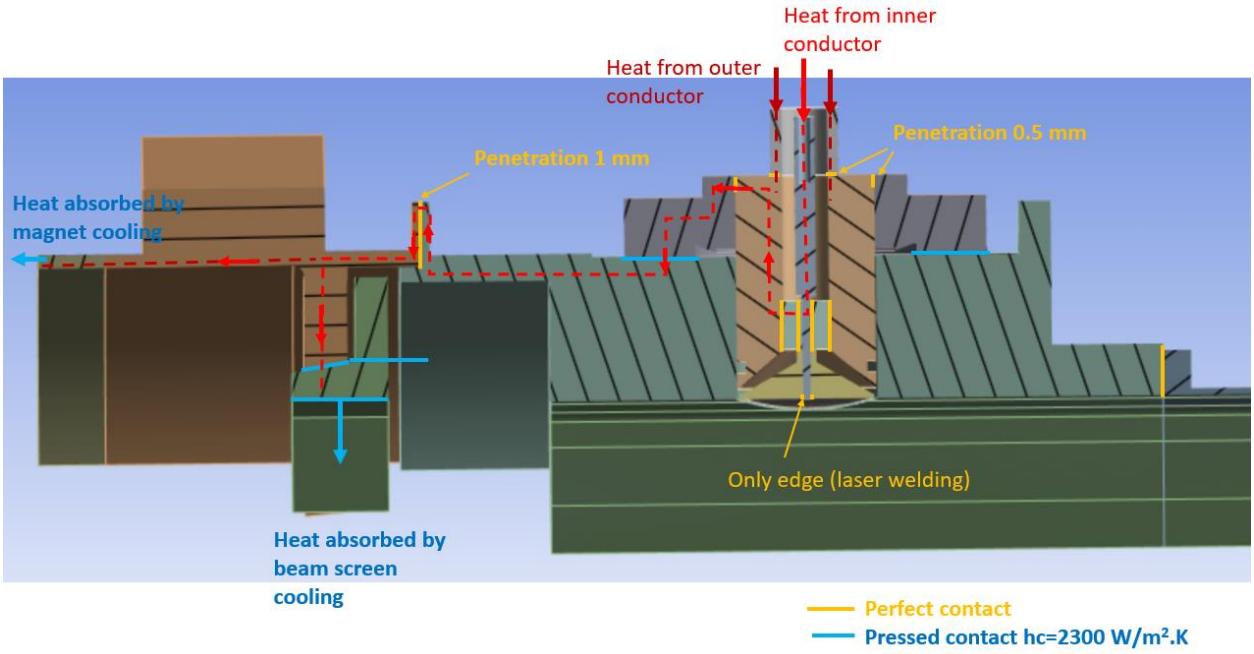


Figure 6 Contact condition in the model and heat propagation path representation.

Boundary conditions

1. Heating: Thermal conduction

The heat coming from the cryostat BPM feedthrough, considered at room temperature (293 K), will be conducted through the cable to the BPM module. The cable is heat stationed to the heat shield (50 K - 80 K depending on the sector) to limit the thermal conduction from the tunnel side to the BPM module (see Annex 5 for details about the heat sink placement).

2. Heating: Beam-induced resistive wall heating

The CST Wakefield Solver is used to simulate the beam-induced resistive wall heating (RWH) from a proton beam with 290 bunches with bunch charge of 30.5 nC and rms bunch length of 6 cm consistent with the high center of mass beam scenario (Ref. [1]). In this CST model, the beam chamber walls are divided in

sectors of 20 degrees to get the local heat distribution for each of these sectors (Fig 7). The heat flux values are scaled for electrical resistivity with a value of ρ = 5E+8 S.m (corresponding to a RRR10 copper).

We will consider that the beam can be offset up to 23 mm horizontally and 2 mm vertically in the BPM (from [7]).

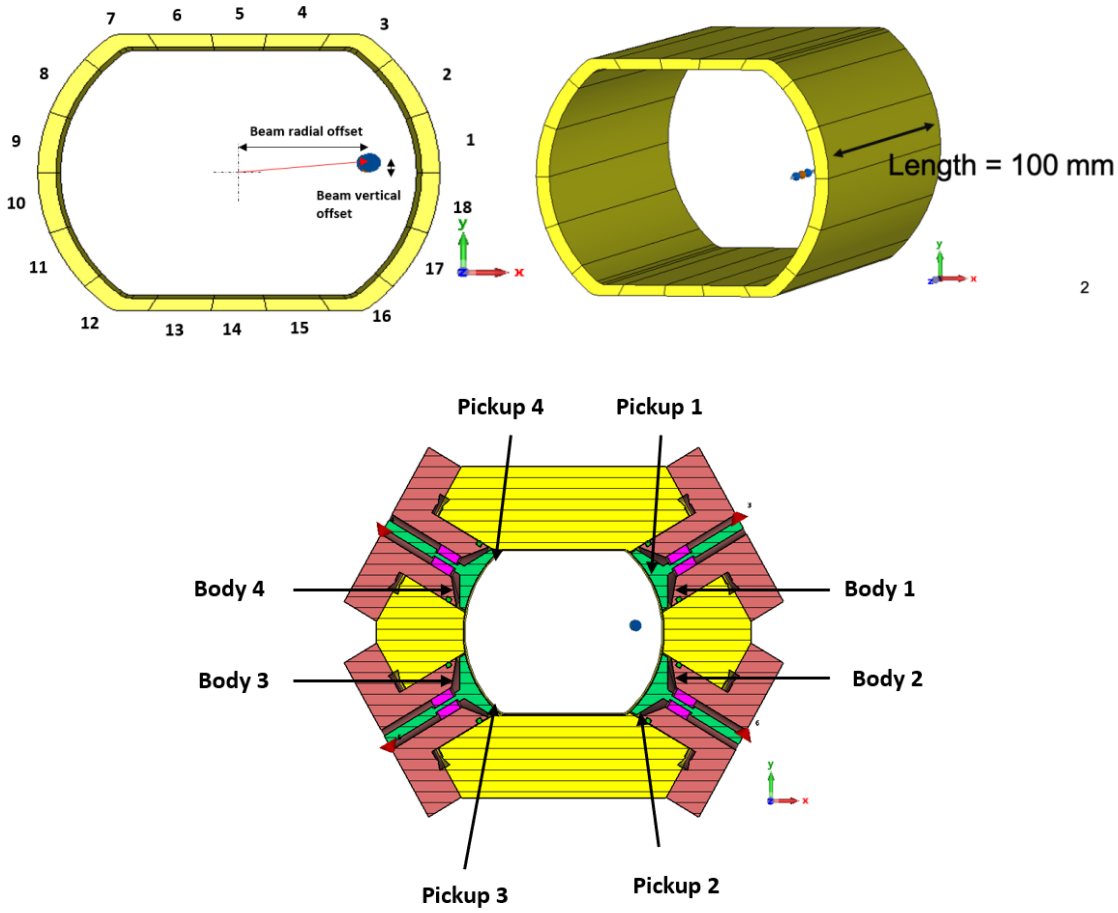


Figure 7 CST model for RWH and beam wall division (top) for pickup and BPM body (bottom)

Table 1 gives the results from this CST simulation on the wall of the beam vacuum chamber.

Table 1 – Heat flow from CST for beam chamber walls - cell empty means a symmetry condition is used

Heat flow by sector for a 150 mm long section (mW)			
Sector ID (see Fig 7)	**Centered beam**	**Offset Radial +20 mm**	**Offset Radial +23mm/Vertical+2mm**
1	1.69	29.24	60.28
2	1.49	7.58	11.01
3	1.16	1.89	1.79
4	3.77	1.85	1.35
5	4.84	0.84	0.53
6	-	0.32	0.19
7	-	0.07	0.03
8	-	0.07	0.04
9	-	0.07	0.03

10	-	-	0.03
11	-	-	0.03
12	-	-	0.03
13	-	-	0.14
14	-	-	0.39
15	-	-	0.82
16	-	-	0.82
17	-	-	4.25
18	-	-	30.09
Total heat RWH (mW)	**42.1**	**83.9**	**111.9**
Equivalent linear heat flux (mW/m)	**281**	**560**	**746**

Another CST model is used to evaluate the power deposited by RWH on the pickup surface as well as the pickup flange (Fig. 7) with the same beam conditions.

Table 2 depicts the heat deposited on the pickup surface and on the BPM flange because of leaking fields through the small gap ~ 250 microns between the pickup electrode (green) and flange (orange). The power deposited on the pickup surface is scaled with an assumption of solid copper (RRR=100).

Table 2 Heat flow from CST for the pickup and flanges –cell empty means a symmetry condition is used

Heat flow (mW)	**Centered beam**	**Offset Radial +20 mm**	**Offset Radial +23mm/Vertical+2mm**
Pickup 1 (Copper)	0.14	0.86	1.30
Body 1 (Stainless steel)	7	42.6	65
Pickup 2 (Copper)	-	-	0.48
Flange 2 (Stainless steel)	-	-	23.9
Pickup 3 (Copper)	-	0.03	0.02
Flange 3 (Stainless steel)	-	3.2	0.2
Pickup 4 (Copper)	-	-	0.02
Flange 4 (Stainless steel)	-	-	0.2
Total resistive wall heating RWH (mW)	**70.7**	**130.6**	**203.0**

3. Heating - Coaxial cable RF heating

The propagation of the voltage signal along the coaxial cable will generate heat by resistive and dielectric heating. A 1D model has been setup to evaluate this heating and the signal attenuation for a given cable temperature profile. This model is described in Appendix I.

The CST model depicted in Fig. 7 is also used to compute the fields excited by the beam, coupled to the BPM pickups and propagating along the coaxial cables (see Fig. 9).

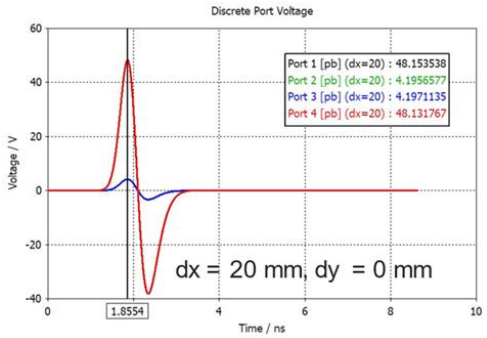


Figure 8 CST simulation BPM electric signal for various beam vertical offsets (radial offset = 20 mm)

Table 3 CST simulation peak voltage for various beam scenario

	Centered beam	Radial +20 mm	Radial +23 mm Vertical +2 mm
Signal peak voltage (V)	19.9	48.2	58.5

This signal is processed by the 1D cable heating model with the cable temperature profile (see Appendix I for more details) and gives a heating profile along the cable length for the resistive and dielectric heating.

The cable will be cooled by conduction only. Overall, its thermal behavior will follow the equation:

$$P_{resistive}(T) + P_{dielectric} - P_{conduction} = 0$$

$$\frac{\Delta x.\sqrt{f.\rho_{i,e}(T)}}{r_{i,e}}.\int i^2 dt + f_b.Z_c.\int i^2 dt.\left(1 - 10^{\frac{-\alpha.\Delta x}{10}}\right) - k(T).2\pi\, r_{i,e}.\frac{\Delta T}{\Delta x} = 0 \qquad - \qquad \text{Eq. (1)}$$

With

- $f\ [Hz]$ - signal reference frequency
- $\rho_{i,e}(T)\ [\Omega.m]$ - resistivity for the inner or outer conductor
- $r_{i,e}\ [m]$ - conductor radius for the inner or outer conductor
- Δx [m] – The length of cable considered
- $\alpha\ [\frac{dB}{m}]$ - cable dielectric loss
- $f_b\ [Hz]$ - bunch revolution frequency
- $Z_c[\Omega]$ - characteristic impedance of the output port.
- $k(T)$ [W/m.K] is the conductor material thermal conductivity
- $S_{i,e}$ [m^2] the cross section of the inner or outer conductor
- $\frac{\Delta T}{\Delta x}$ [K/m] the temperature gradient along the cable

More details on this approach can be found in [8].

4. Heating – Pickup stem heating

The pickup stem is currently planned to be made of Inconel. So its resistivity is higher than the copper conductor of the coaxial cable. This is computed as follows:

$$R(T) = \rho(T).\frac{l}{2.\pi.r.\delta(T)}$$

With:

$$\delta(T) = \sqrt{\frac{2.\rho(T)}{\mu_0.2.\pi.f}}$$

The term $\rho(T)$ is evaluated for the temperature of the connection with the coaxial cable inner conductor. Overall, this represents 15-20 % of the total cable RF heating.

Table 4 Coaxial cable and stem heating and attenuation for different beam offset

	Centered beam	Beam offset - radial +20mm	Beam offset - Radial +23mm Vertical +2mm
RF signal peak voltage (V)	19.9	48.2	58.5

Max signal RF power (W)	0.087		0.51		0.75	
Cable type	0.141”	0.090”	0.141”	0.090”	0.141”	0.090”
Max cable heating (mW)	5.2	7.2	30.5	44.9	45.0	125
Cable attenuation (dB)	-0.265	-0.373	-0.267	-0.400	-0.267	-0.395
Stem heating (mW)	4.6		4.6		12.9	

Table 4 shows the overall cable heating obtained through the 1D model. Max RF power and Max heating is the value for the pickup closest to the beam (for example Pickup 1 on Fig. 8).

5. Electron clouds heating

Electron clouds heating has been computed in Ref. [9]. Fig. 9 represents the electron cloud heating expected in the interconnect region (no magnetic field) for various Secondary Electron Yield (SEY) values of the beam wall surface.

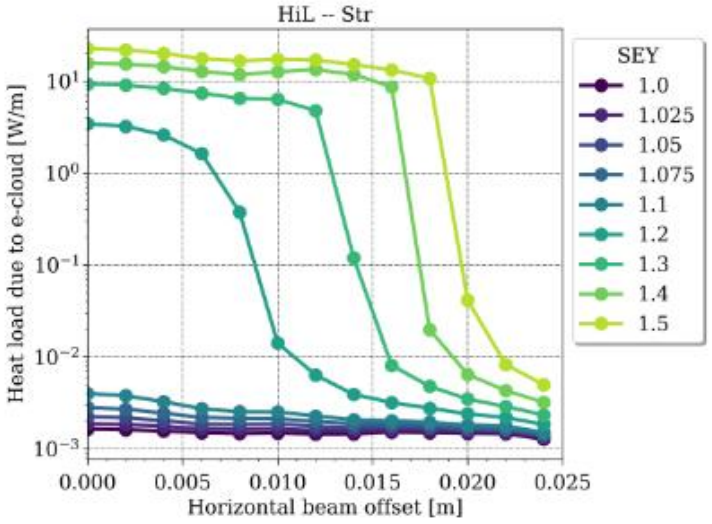


Figure 9 Electron cloud heating vs. SEY. Adapted from [9]

6. Cooling – beam screen cooling circuit

Fig.3 shows that the beam screen is pressed onto by the cooling jaw. The cooling jaw and beam screen are both metallic surfaces, so this is treated as a thermal contact conductance (TCC). The applied interface pressure with the current bolting pattern is estimated in the 40-60 MPa range at 2/3 of the bolt elastic limit. With a Fukuoka correlation this gives TCC values in the range 2400-3300 W/m^2.K.

We applied 2400 W/m^2.K (see Fig. 6) conservatively.

Note: Effective TCC are notoriously difficult to predict. Especially on large planar surfaces. So, for robustness, the implementation of an alternative load path is desirable as laid out in section i).

7. Cooling – magnet cooling line

The BPM interconnect module will be welded onto the end of the stripline BPM module. Some of the heat from this BPM module will be conducted to the magnet helium through the outer walls of the stripline BPM. A dedicated FE study of the stripline BPM obtained the equivalent thermal resistance of this

conduction. This equivalent thermal resistance is implemented in the model as a solid with thermal conductivity worked out to represent the stripline BPM conductance (see Fig. 4).

8. Cooling – Heat shield heat stationing

To limit the conduction from the tunnel temperature to 4K, the BPM cables are heat stationed to the heat shield (50-80 K). The position of this heat station has been chosen to minimize the cryoplant operating cost (see Appendix IV for details). The model considers a heat extraction with a convection coefficient representative of the heat shield thermal resistance (details can be found in appendix VII) with a temperature of to 80 K, 350 mm after the tunnel feedthrough and for a length of 100 mm.

9. Cooling - Additional heat stationing

A subsequent study evaluated the advantage offered by heat stationing the BPM module to the beam screen cooling circuit with thermal straps (copper or aluminium braids).

These boundary conditions were treated as convective coefficient representative of thermal straps thermal resistance (47 K/W for strap reference 69925K32). They were placed on the top and bottom of the BPM module between two pickups.

Fig. 11 shows a schematic summary of the boundary condition discussed here.

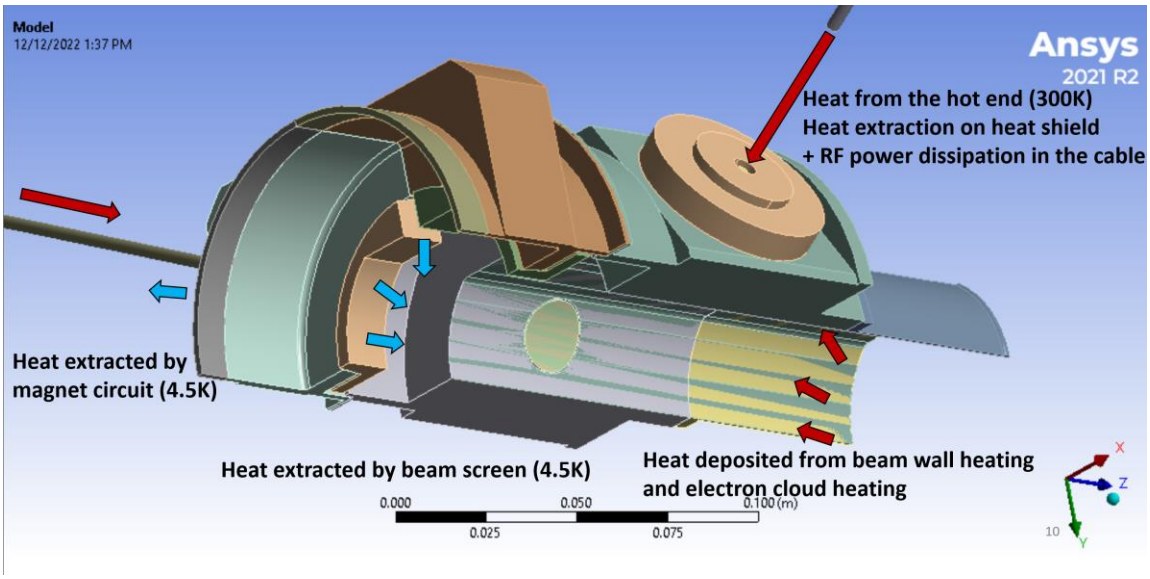


Figure 10 Summary of the boundary conditions for the thermal simulation

The FE model has been uploaded on the BNL database and is available - Ref. [11].

Results and discussion

1. Nominal case

Fig. 11 shows the thermal distribution on the HSR BPM module using the coaxial cable dimensions of 0.141” for the centered beam.

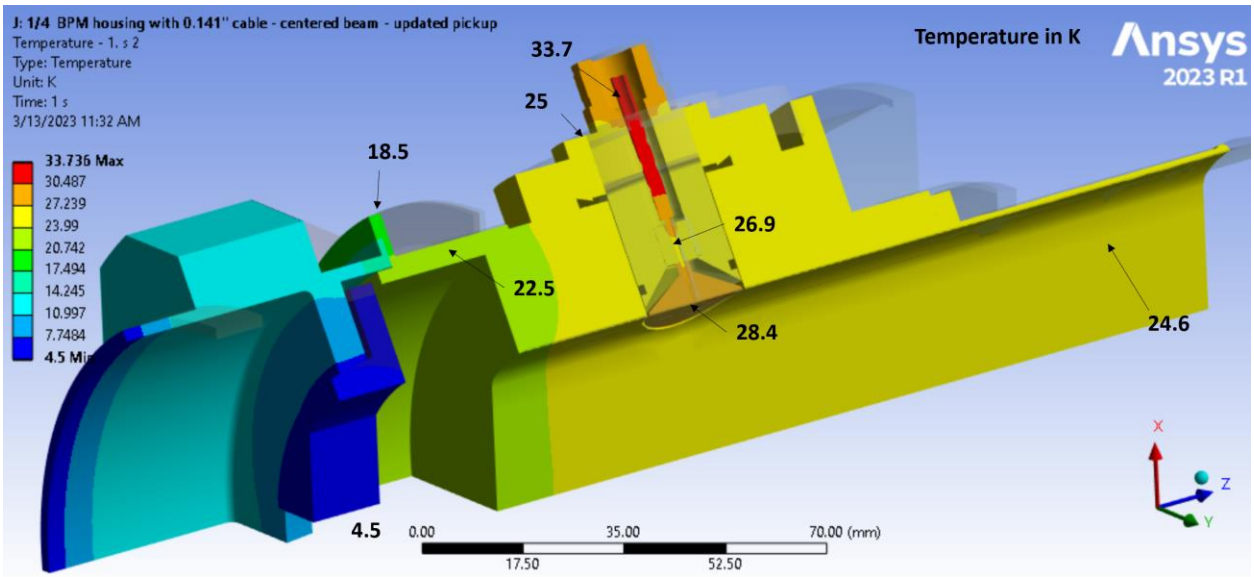


Figure 11 Cross section view of the FE model results for the 0.141” cable in the centered beam scenario.

In this case, the RWH is low (71mW - see Table 2 – Fig 13 case 2) and the main source of heating is from the cable conduction from the tunnel feedthrough (see Fig 11 – case 2). The following results will be sorted by heating case. Table 4 present the different conditions for the scenario simulated.

Table 5 Summary of the simulation scenario

Case	Conditions
1	0.141" cable - No beam
2	0.141" - Centered beam SEY 1.14 (see section 5.2)
3	0.141" - Centered beam SEY1.2 (see section 5.2)
4	0.141" - Offset beam R+20mm
5	0.141" - Offset beam R+23V+2mm
6	0.141" - Offset beam R+23V+2mm with module anchoring
7	0.090" cable - No beam
8	0.090" - Centered beam SEY 1.14 (see section 5.2)
9	0.090" - Centered beam SEY 1.2 (see section 5.2)
10	0.090" - Offset beam R+20mm
11	0.090" - Offset beam R+23V+2mm
12	0.090" - Offset beam R+23V+2mm with module anchoring

Fig. 12 represents the model power input and output for each simulated scenario described in Table 4.

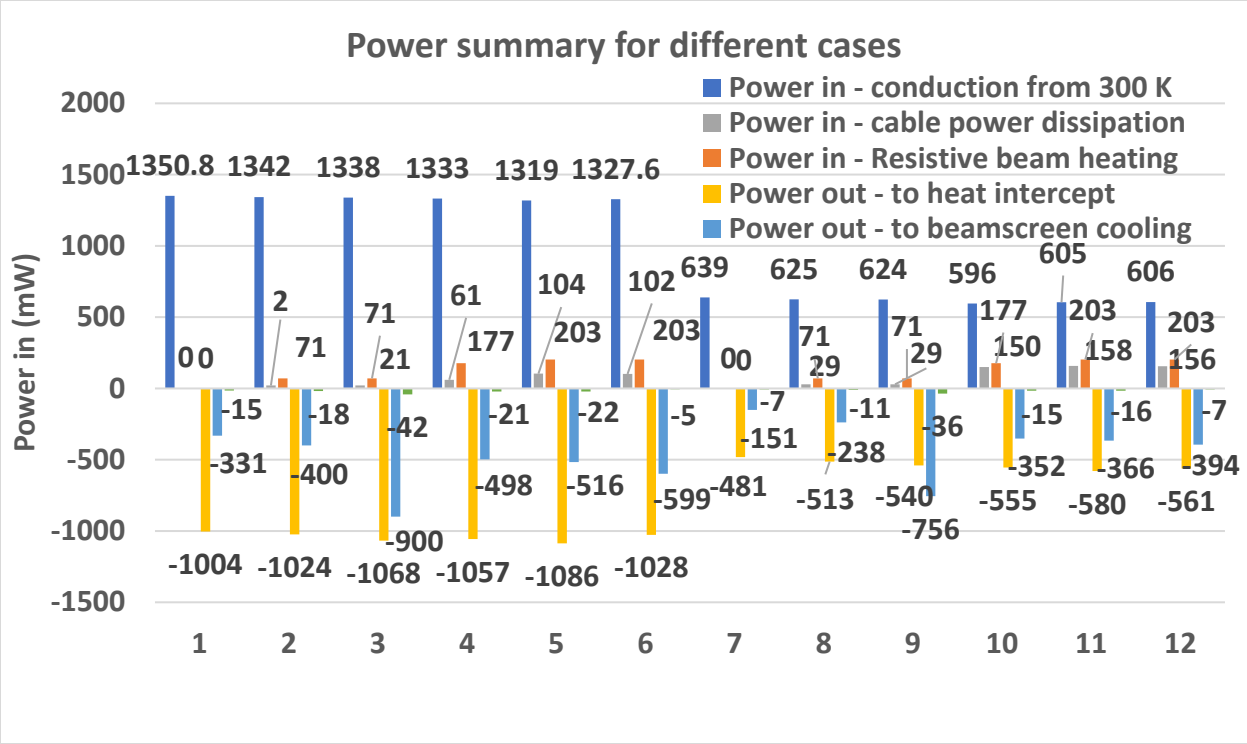


Figure 12 Summary of power distribution for the different cases for a 4x cable BPM module

The power summary from Fig. 13 shows that for the 0.141" cable, the dominant source of heat is the tunnel feedthrough conduction. Most of this heat is intercepted by the heat shield stationing. However, even without beam (Fig 13 - case 1), the heat flux to the 4 K beam screen remains at 331 mW (516 mW with an offset beam at high intensity – case 5). The smaller 0.090" cable (case 7) allows a reduction of conducted heat flux to the beam screen to only 151 mW (case 7). When using the smaller 0.090" cable, the signal attenuation increases however (see table 3).

Fig. 13 shows a summary of the temperature reached on the BPM button face and the beam enclosure wall in the different cases.

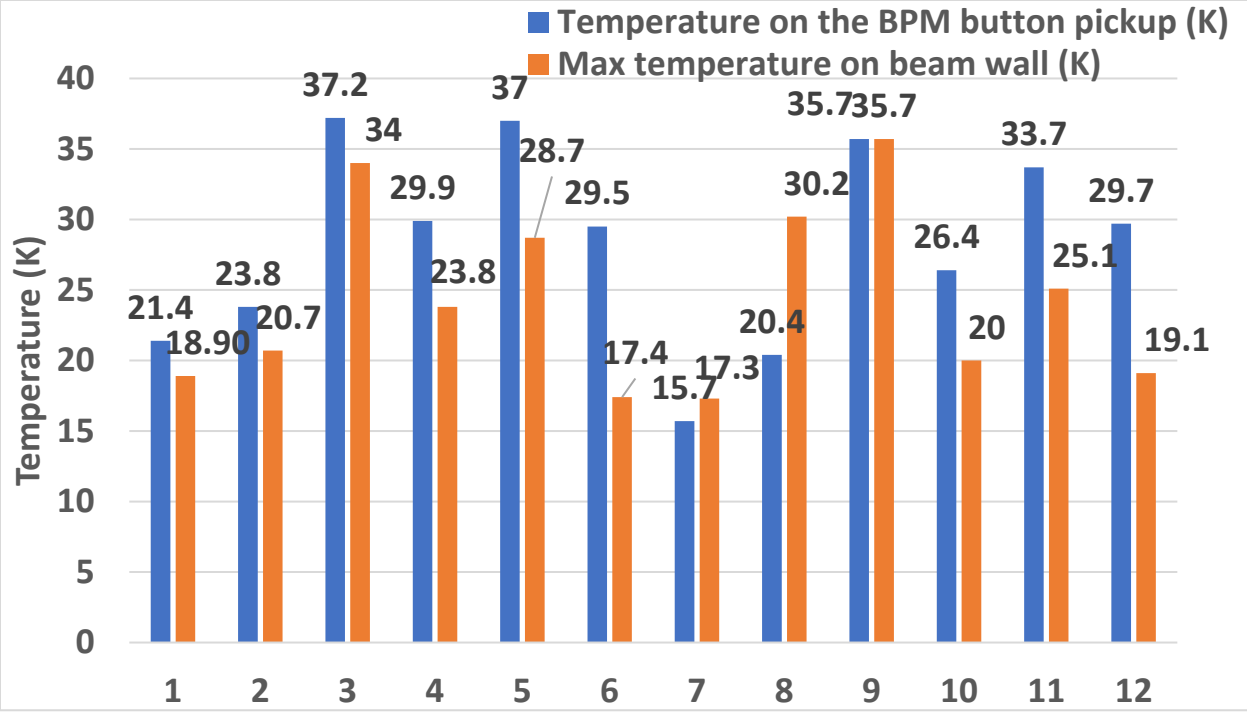


Figure 13 Summary of max temperature for different cases

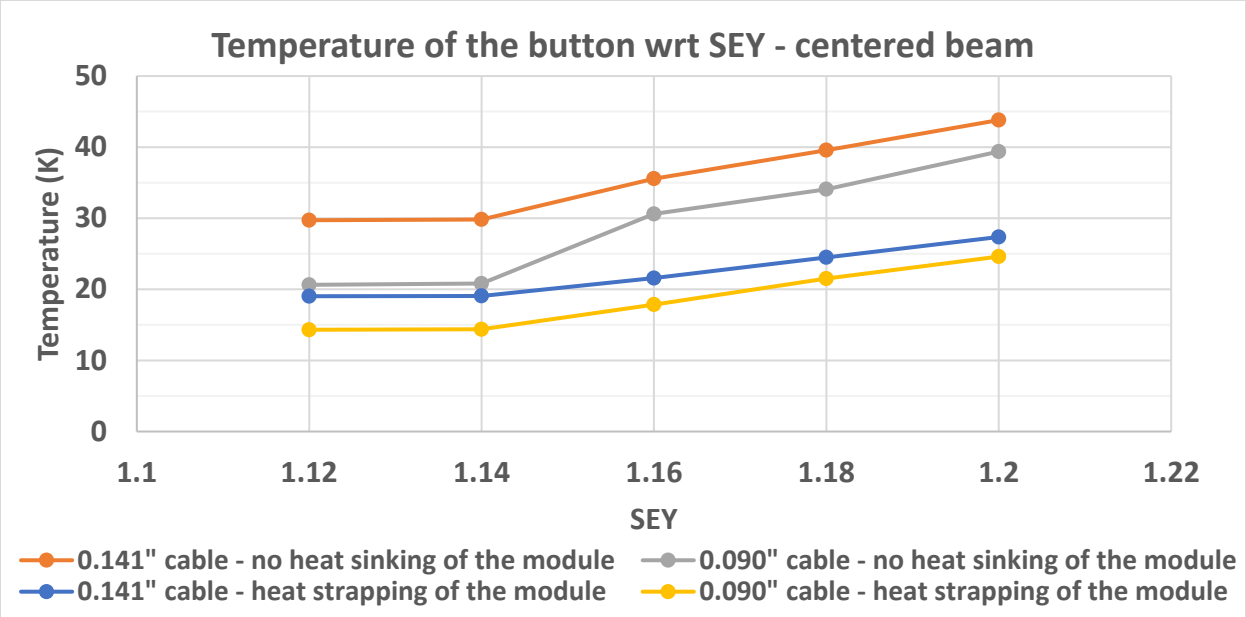
A maximum temperature of 37.2 K is found on the BPM button face (Fig 14 - case 3) with the BPM module wall kept around 34 K. All other cases have lower temperature.

Since the BPM pickup is coated with amorphous carbon coating to limit the SEY, a higher level of gas cryogenically adsorbed is expected compared to bare metallic surfaces. To limit the release of this condensed gas with the beam heating, the temperature of the walls should be contained under 40 K [10]. This is achieved by the current design although by a narrow margin (Fig. 14).

Heat stationing the BPM module itself is an efficient method to reduce the beam wall temperature (see Fig 14 case 6,12). The tradeoff is a slight increase in cryogenic power to the beam screen cooling (see Fig. 13 case 6,12).

2. Electron cloud heating study

A dedicated analysis was done to study the effect of Secondary Electron Yield (SEY) on electron cloud heating. As seen on Fig 9 the electron cloud heating is only significant with the centered beam and it will decrease when the beam is offset. So, we will focus on the centered beam scenario. SEY values have been swept from 1.12 to 1.2 and resulting temperature are plotted for the vacuum beam walls and button surface (Fig 15).



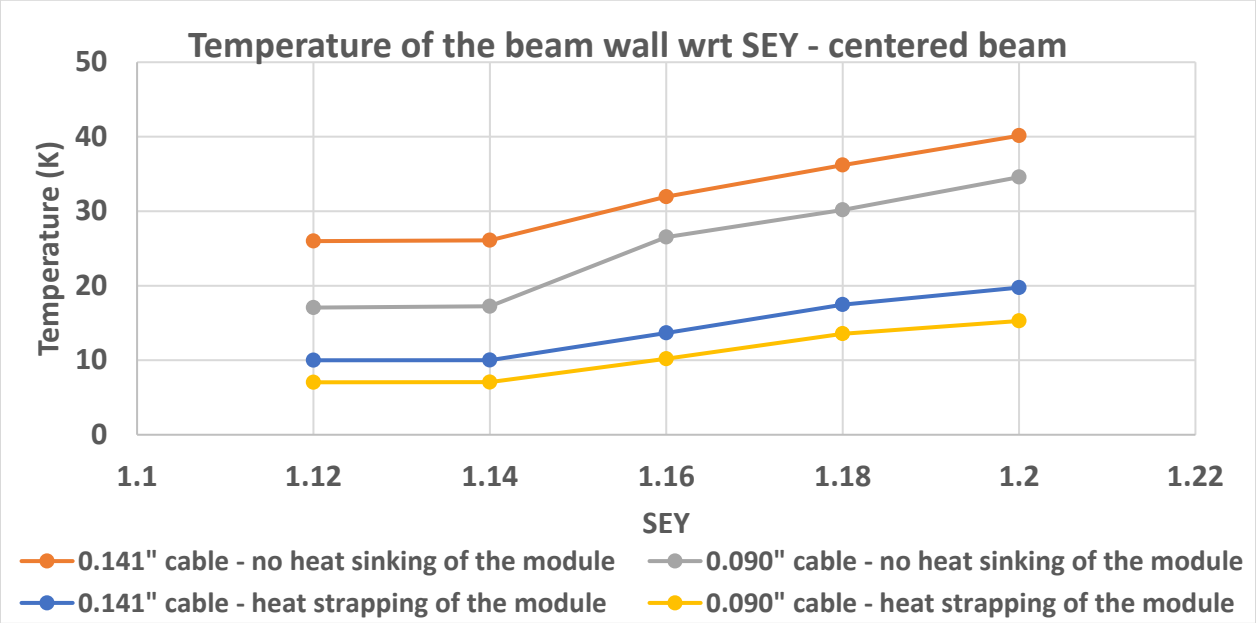


Figure 14 Button (top) and beam wall (bottom) temperature versus SEY

We see no significant temperature difference between SEY 1.12 and SEY 1.14 so keeping a SEY below 1.14 means that no significant heating is generated. This is consistent with Fig. 10.

3. Stress test – higher RF voltage

An analysis with higher RF peak voltage has been conducted and reported in [8]. See Fig 15 for the cable temperature.

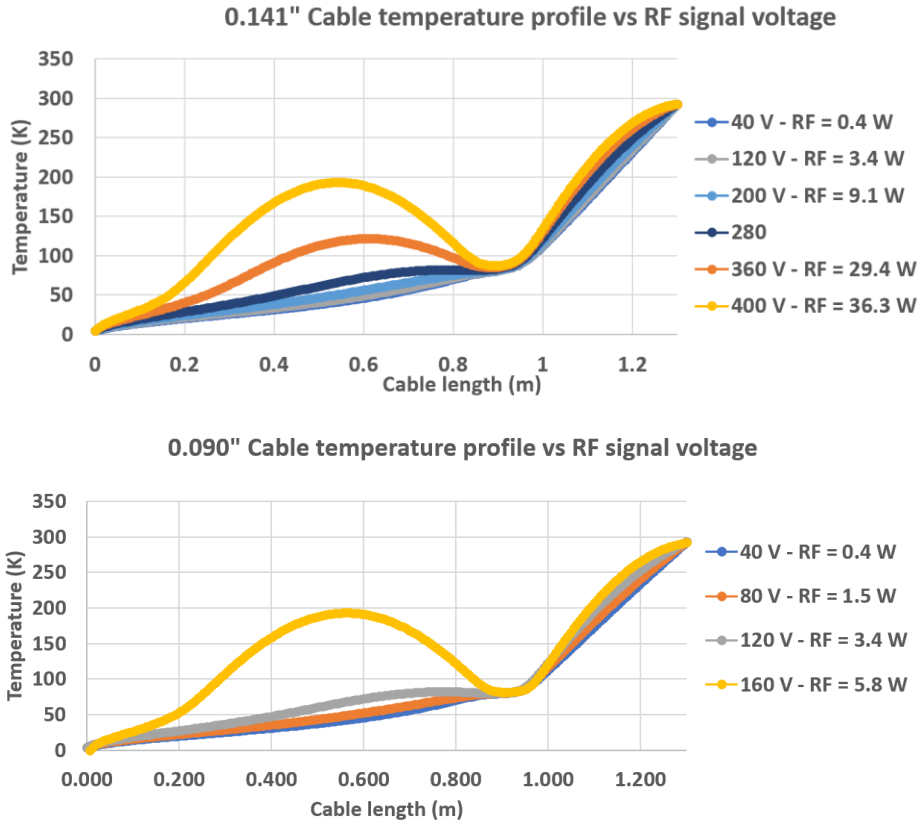


Figure 15 Temperature profile for various RF signal power for (top) 0.141" cable (bottom) 0.090" cable

Since the 0.141” cable has more copper content it is better able to extract heat before its temperature rises significantly. However, even for the 0.090” this temperature elevation only becomes significant above 120 V and the maximum peak voltage expected for the HSR is 60 V (see table 3).

Note: 120V corresponds to over 4x the RF power and dissipated heat at 60V ($P \propto V_{RF}^2$).

4. Lifecycle evaluation of using the 0.090” cable versus the 0.141”

As seen of Fig. 13, the smaller 0.090” coaxial cable brings less heat to the cryogenic circuits. We estimate the average saving to be around 150 mW per interconnect to the 4.5K helium circuit and 500 mW to the 80-50K heat shield circuit (see Fig. 13). There is an estimated 246x interconnects total. With the cryogenic efficiency expected in [5] estimated energy saving is 70.1 MWh per year. Assuming an average electricity cost of 0.1 $/kWh this equates to $7,010/year or $140,000 saved on the operating budget over the 20 years EIC project.

Conclusion

A thermal model to simulate the new HSR interconnect BPM has been setup and used in a variety of load cases. In the heating case expected for EIC operation, the expected heating of the BPM module beam surface is limited to less than 30 K and 40 K on the button itself.

The use of two different cables (0.141" and 0.090") has been evaluated and for cryogenic purposes the smaller has better thermal performance with the tradeoff of a slightly higher RF attenuation. Both cables are expected to perform adequately otherwise.

The power extracted by the beam screen cooling circuit has been evaluated and a method to heat station the BPM module directly to the beam screen cooling pipe (or manet cooling pipe) has been proposed as an effective way to limit the BPM module temperature elevation and make the cooling scheme more robust.

The FE model generated has been archived and is available for future use (See [11]).

Acknowledgment

The author wishes to thank David Gassner for his precious input and for reviewing this report. Medani Sangroula for providing all CST simulations described here. Jonathan Bellon, Charlie Hetzel, Douglas Holmes, David Gassner, Rob Hulsart, Igor Pinayev, Vadim Ptitsyn, Joseph Tuozzolo and Silvia Verdu-Andres for giving inputs throughout this work.

References

[1] F. Micolon et al., "From RHIC to EIC hadron storage ring - overview of the engineering challenges", in Proc. IPAC'24, Nashville, TN, May 2024, pp. 951-954. doi:10.18429/JACoW-IPAC2024-TUBD1

[2] P. Cameron et al. "RHIC Beam Position Monitor Assemblies" *Proceedings of International Conference on Particle Accelerators*, Washington, DC, USA, 1993, pp. 2328-2330 vol.3, doi: 0.1109/PAC.1993.309311.

[3] P. Thieberger et al. "HIGH INTENSITY RHIC LIMITATIONS DUE TO SIGNAL HEATING OF THE CRYOGENIC BPM CABLES" Conference: Particle Accelerator Conference 2013

[3] S. Verdú-Andrés *et al.*, "A Beam Screen to Prepare the RHIC Vacuum Chamber for EIC Hadron Beams: Conceptual Design and Requirements. doi:10.18429/JACoW-IPAC2021-TUPAB260

[4] F.Micolon et al. "Thermal simulation of the EIC HSR interconnect module - RF fingers" BNL Technical note – BNL-225645-2024-TECH / EIC-ADD-TN-095 (May 2024) - https://doi.org/10.2172/2367449

[5] F.Micolon et al. "Estimate of the marginal cost of cryogenic heat budget for EIC" BNL Technical note – BNL-224168-2023-TECH

[6] V.Baglin et al. "Cryopumping and vacuum systems » Proceedings of the 2017 CERN–Accelerator–School course on Vacuum for Particle Accelerators, Glumslöv, (Sweden)

[7] Minute of the 16th Dec 2022 meeting on worst HSR BPM beam misalignment – available (internal BNL) : https://brookhavenlab.sharepoint.com/:u:/r/sites/eRHIC/HSR%20BPM/Shared%20Documents/Tech%20note%20draft/Minute%20RE%20Discussion%20on%20worst%20HSR%20BPM%20misalignment.msg?csf=1&web=1&e=tgXhWf

[8] F.Micolon et al. "Thermal engineering of the cryogenic beam position monitors for the EIC hadron storage ring" Cryogenic engineering conference (CEC23) proceedings. DOI 10.1088/1757-899X/1301/1/012152

[9] S. Verdú-Andrés *et al.*, "Electron cloud thresholds at the arcs of the Electron-Ion Collider hadron storage ring" - Technical note: BNL-224588-2023-TECH

[10] R. Salemme et al. "Vacuum Performance of Amorphous Carbon Coating at Cryogenic Temperature with Presence of Proton Beams", in Proc. 7th Int. Particle Accelerator Conf. (IPAC'16), Busan, Korea, doi:10.18429/JACoW-IPAC2016-THPMY007

[11] FE model archive available – EIC Windchill : Products > ELECTRON ION COLLIDER > DOCUMENTS > CALCULATIONS > 2551_HSR BPM

Appendix I - Evaluating the loss in a cryogenically cooled RF coaxial cable.

Introduction

A coaxial cable carrying a RF signal power will be heated by attenuation. In the case of the BPM coaxial cables, these are surrounded by vacuum which suppresses convective cooling. The only way to evacuate its generated power is conduction which implies a temperature elevation of the cable.

The RF heating power is often made available by the cable manufacturer at room temperature. However, the cryogenic losses are significantly different from the room temperature losses, and this is less frequently documented. Our aim is to get a tool that described the losses occurring in a coaxial cable for a given temperature profile and a given RF signal propagation. We will aim to discuss the model principles in this section.

Model principle

A finite difference 1D model is used to compute the resistive losses along the cable. These resistive losses are a function of the conductor material resistivity (temperature-dependent) and the conductor skin depth (dependent on frequency of the RF signal and the resistivity – so temperature).

This 1D model takes an initial temperature profile and will compute the loss in each segment of the cable. This can be used as an input to the ANSYS model containing all relevant boundary conditions. We can compare the new cable temperature profile with the one previously used for the cable heating model. If the temperature profiles are close, the result is considered as converged. If not, another iteration is run until the result is converged.

Fig. 17 describes schematically the steps of the simulation process:

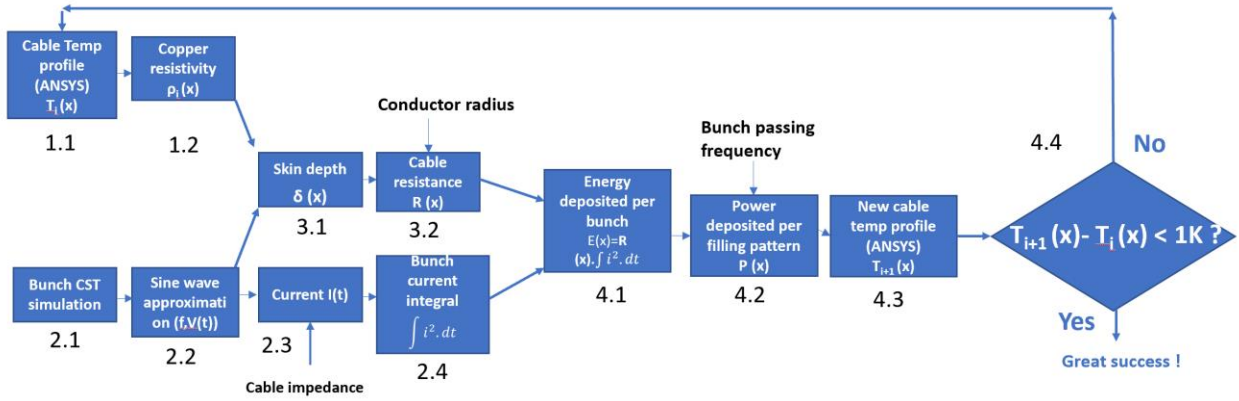


Figure 16 Cable RF loss simulation process

The same process is done independently for the inner and outer conductor.

We will describe the operation done at each step described in the graph Fig. 17 :

Step 1.1

We get a discretized temperature profile of the cable length from a previous ANSYS iteration (or we can manually input a guess). *Note: A good starting point for the EIC cable simulation is the conduction only cable temperature profile or a point with a similar dissipated RF power.*

Step 1.2

The cable temperature profile is translated into a copper resistivity for each cable segment.
Note: the copper resistivity is dependent on RRR below 30 K only. Otherwise, it can be considered independent.

Step 2.1

We get the bunch RF time-dependent signal voltage $V(t)$ from the CST simulation.

Step 2.2

We can determine the CST bunch signal energy ($E = \frac{1}{R}.\int V(t)^2.dt$) and approximate this bunch with a sine signal of similar frequency. Then we adjust the amplitude to get an identical signal energy.

Note: the frequency approximation is used to work out the propagation skin depth (step 3.1). A higher frequency means a smaller skin depth (so higher cable heating). The reference frequency for room temperature has been determined to be around 660 MHz (see annex 2 for details). We initially selected a frequency of 1 GHz. This is conservative, with around 20% higher heating power.

Step 2.3

We can now extract the current integral from the sine approximation with the hypothesis that the match load is 50 ohms.

Step 2.4

We integrate this current squared.

Step 3.1

The skin depth is a function of resistivity and signal frequency:

$$\delta(x) = \frac{1}{2.\pi}\sqrt{\frac{\rho(x)}{f}}$$

Step 3.2

The cable resistance R(x) is a function of the cable geometry (radius of the conductors), skin depth and resistivity:

$$R(x) = \rho(x).\frac{\Delta x}{2.\pi.r.\delta(x)}$$

Step 4.1

We will now work out the power dissipated per bunch passing:

$$\text{E(x)=R (x)}.\int i^2.dt$$

Step 4.2

Knowing the machine filling pattern, we know how many bunches the BPM will see per second. With the 30.5 nC 6 cm RMS bunch we expect a maximum machine filling of 290 bunches (out of 315 buckets). With a bunch revolution period of 12.8 us this gives a bunch passing frequency of 22.7 MHz.

We can then multiply the energy deposited by bunch E(x) with the bunch passing frequency to get the deposited power P(x).
Note: the underlying assumption is that we can approximate a succession of bunches as a constant heating power by averaging. This has been validated with a transient simulation.

Step 4.3

This power generated by the bunch RF signal is imported in ANSYS as a convection coefficient on the conductor surface. The ANSYS simulation is run with these new parameters.

Step 4.4

We can compare the cable temperature profile used to generate the previous iteration with the new cable temperature profile from step 4.3. If it differs by more than 1K the whole iteration must be repeated with this new temperature profile, as a higher cable temperature will mean a higher generated power. If not we will consider the solution as converged and acceptable.

A coaxial cable RF loss is composed of the resistive losses, computed above and the dielectric loss resulting from the motion of charges through the dielectric (then acting like a capacitor). These are usually neglected at low frequency, however at 1 GHz they should be included.

The dielectric loss, although a minor portion of the overall RF loss, is computed using the manufacturer formula for room temperature. Knowledge of the evolution of the dielectric loss for sintered SiO2 at lower temperature has not been found in the literature.

Manufacturer's attenuation formula at room temperature for the 0.141" cable :

$$a(\frac{dB}{100ft}) = 0.2923.\sqrt{f(MHz)} + 0.0011 * F(MHz)$$

Manufacturer's attenuation formula at room temperature for the 0.090" cable :

$$a(\frac{dB}{100ft}) = 0.5642.\sqrt{f(MHz)} + 0.0011 * F(MHz)$$

Appendix II – Determination of the reference frequency for attenuation

CST studio is used to determine the bunch signal voltage. This voltage profile has a similar pattern irrespective of the bunch position within the beampipe (the bunch position offset will mostly affect the signal voltage).We can then use the Fourier transform of this voltage to study the frequency composition of the EIC bunch pattern.

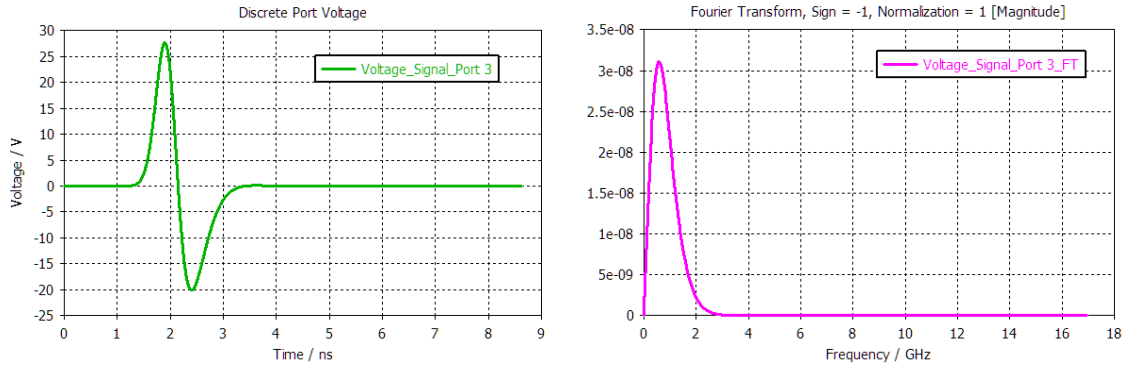


Figure 17 CST simulation of a 30.5 nC, 6 cm centered EIC bunch (M.Sangroula)

The bunch RF signal power distribution can be obtained by multiplying the Fourier transform of the voltage by that of the current. Since voltage and current are in phase the pattern is similar to figure 19.

The cable attenuation has a resistive ($\propto \sqrt{f}$) and dielectric loss ($\propto f$). The manufacturer specifies coefficient for both contribution.

$$\alpha(f) = a.\sqrt{f} + b.f$$

Attenuation (dB/100 ft)	a	B
0.090” cable	0.5645	0.0011
0.141” cable	0.2923	0.0011

We can then convolute the FT from the EIC bunch pattern to the cable attenuation to get an image of the cable loss vs. frequency for the EIC bunch signal. And from there we can plot the power integral for these FT (see Fig. 19).

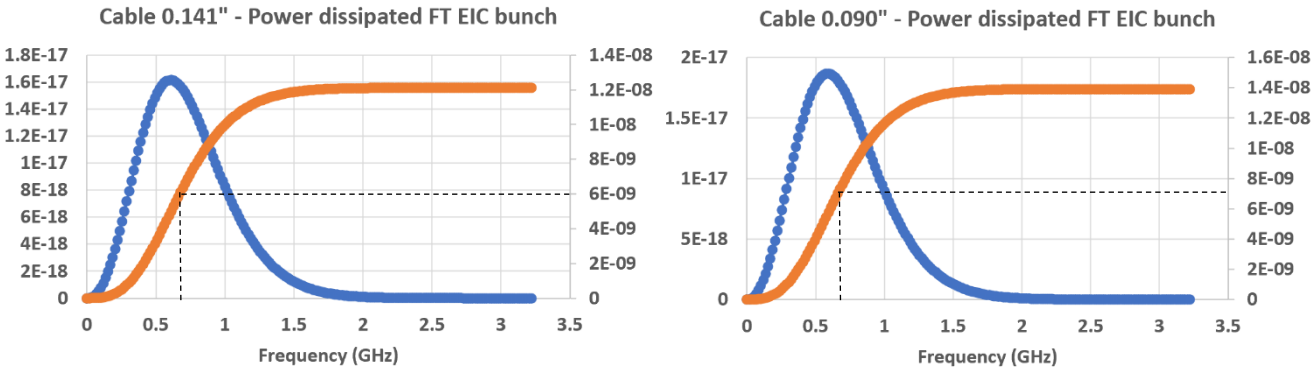


Figure 18 Attenuation vs frequency for the EIC centered bunch RF signal through the 0.141" (left) and 0.090" (right) SiO2 cables

As seen on figure 2, the frequency of median power dissipation is around 660 MHz. The same amount of power is dissipated at higher and lower frequency so this can be used as an average frequency to simplify further analysis.

Note : the attenuation characteristic used is given at room temperature. Its evolution at lower temperature is essentially linear (see annex IV) so this conclusion should be reasonable even at lower temperatures.

Appendix III – Comparison of the coaxial loss model with published data from the LHC

1. Introduction

To assess the reliability of the 1D model used to compute the RF losses along the BPM cables, we have compared its results to data available in the literature. An example of such data that is sufficiently detailed and in a relevant configuration is the paper from C.Bovet et al. “Measurement and modelling of the thermal dissipation of a cryogenic coaxial cable for LHC BPMs” (link).

In the following section we will compare the results from our simulation to the experimental results contained in the paper.

2. Simulation setup

a. Geometry

To follow the conditions described in [1], we have made a FE model containing a 0.65m coaxial cable. The cable is made of an inner conductor made from stainless steel with a copper cladding. The dielectric is made from sintered SiO2 with an estimated density of 12.8%. The outer conductor is made from a stainless-steel jacket with an inner cladding of copper. The copper cladding is considered as having a RRR30 (see section “evaluating the copper cladding RRR”).

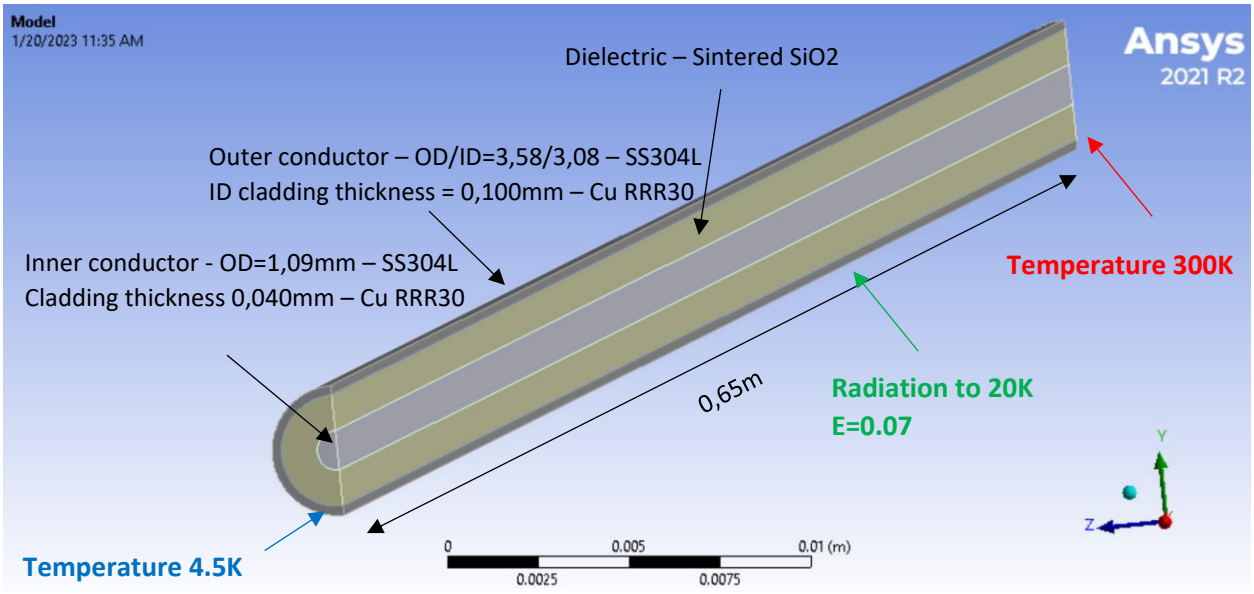


Figure 19 FE Model geometry, materials and boundary conditions

b. Boundary condition

The hot end of the cable is considered at 290K while the cold end is fixed at 4.5K.

The outer jacket of the coaxial cable will radiate in the thermal shield enclosure that is cooled at 20K. The emissivity retained for the stainless steel outer jacket is 0.07 (Ref.[2]).

The RF power dissipation will be computed using the 1D model. The reference frequency is 390 MHz as indicated in [1].

3. Results and discussion

i. Temperature profile

The cable temperature profile has been computed for three different RF power rating : 0W (conduction only), 10W and 20W included in [1].

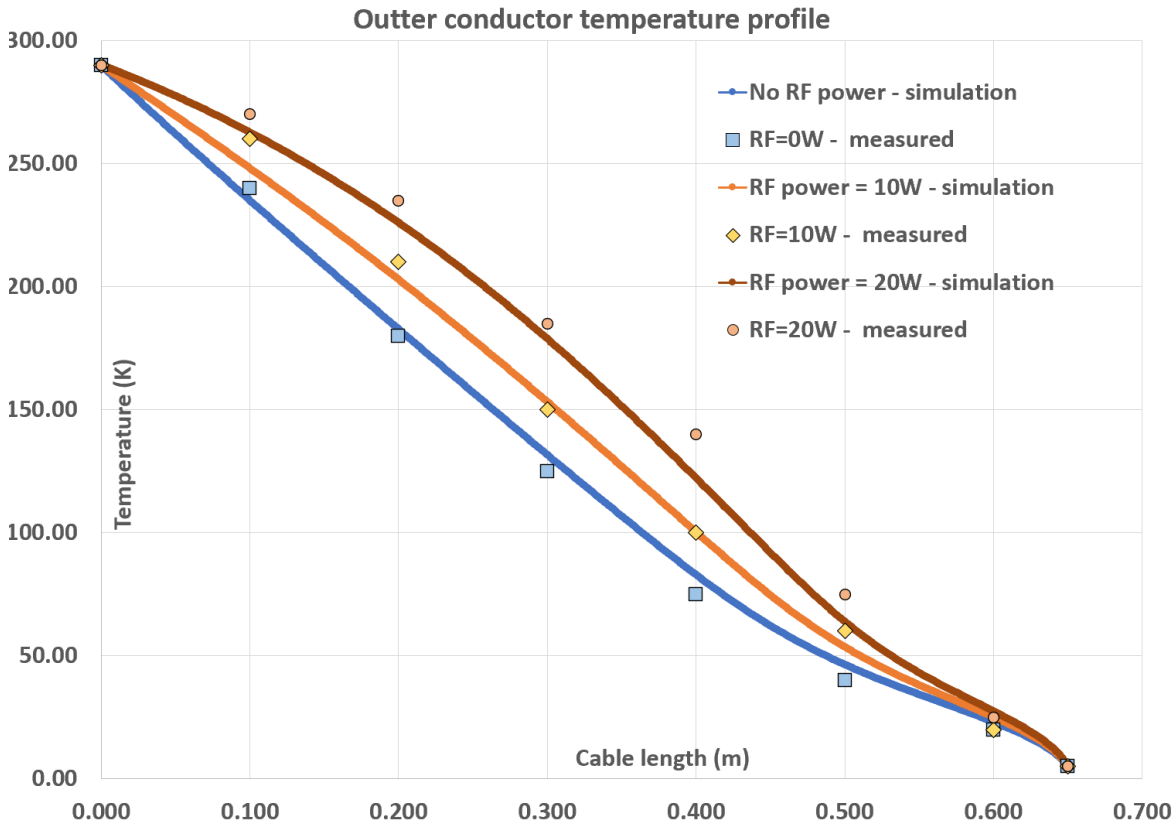


Figure 20 Comparison of measured/simulation temperature profile for various RF power

Overall, the evolution of the temperature profile is consistent with the experimental data. At mid cable (L=0.3 m) the temperature elevation for a P(RF)=20W is +60K measured and +47K simulated.

The mismatch observed, may be due to the room temperature elevation, the geometry of the cable being slightly different in the simulation than reported in [1] or the evaluation of the stainless emissivity that is likely to vary with temperature (considered constant at 0.07 in the simulation).

ii. Power evaluation

The paper [1] also reports on direct RF power dissipation evaluation on the cooled cable. On the graph Fig. 4 we will compare the values measured to the values obtained by simulation.

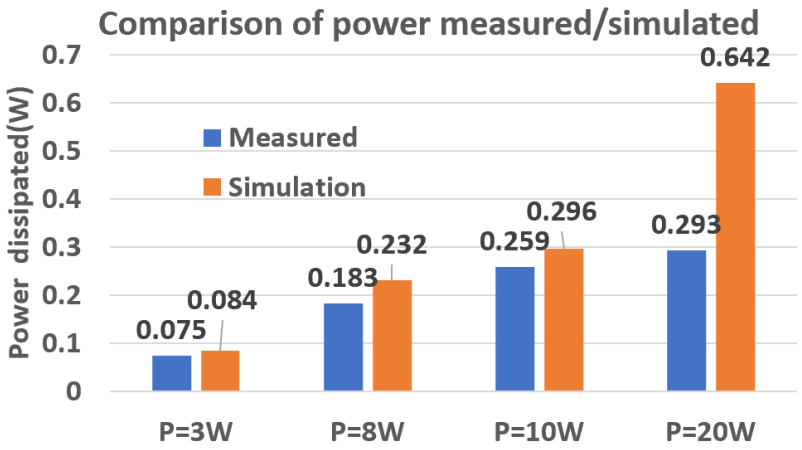


Figure 21 Comparison of measured/simulation values for the RF power dissipation.

The simulated values closely match the measured values for RF power of 3W, 8W and 10W while being consistently slightly overestimated. The measured value for RF=20W (293 mW) is an outlier as mentioned in the paper [1]. It would correspond to an attenuation being halved abruptly instead of the expected linear increase.

To confirm this hypothesis, the evolution of the outer jacket temperature profile (see Fig 3) is coherent to a RF power dissipation being about double at P=20W than at P=10W (about the same temperature difference between P=20W than at P=10W as between P=10W and P=0W).

4. Conclusion

The comparison between the simulated and measurement for the LHC type cable is consistent. The simulated temperature profile elevation for the cable is slightly underestimated. However, the power dissipation evaluation is consistent between simulation and measurement and the simulation seem always slightly conservative which is reassuring.

Reference

[1] C.Bovet et al. “Measurement and modelling of the thermal dissipation of a cryogenic coaxial cable for LHC BPMs” LHC project Note 79 - link

[2] J.Ekin “Experimental techniques for low-remperature measurements” Physics Today **60**, 5, 67 (2007); https://doi.org/10.1063/1.2743130

Appendix IV – Comparing the simulated attenuation to the manufacturer data

1. Introduction/context

At a later stage during this work, we managed to obtain cryogenic attenuation results from a potential cable manufacturer company. We will report them here and describe how they compare with the data we have simulated previously.

2. Precisions on manufacturers data

The data obtained from the manufacturer did not describe the test setup in detail. After enquiry, the cable length used was close to 5 feet. We assume the temperature to be constant along these 5 feet without considering any end effects. Any warmer ends would tend to give a higher attenuation but without knowing the setup details this cannot be estimated accurately.

The temperature tested ranged from 20 degC to -180 degC (~100K). The frequency tested ranged from 200 MHz to 1 GHz.

We have used our 1D cable model to work out the attenuation in the same conditions. While the resistive losses are evaluated at the relevant temperature the dielectric losses are considered as temperature independent in the 1D model and are always equal to the formula given by the manufacturer for their cable at room temperature (see Appendix I).

3. Results and discussions

a. Attenuation

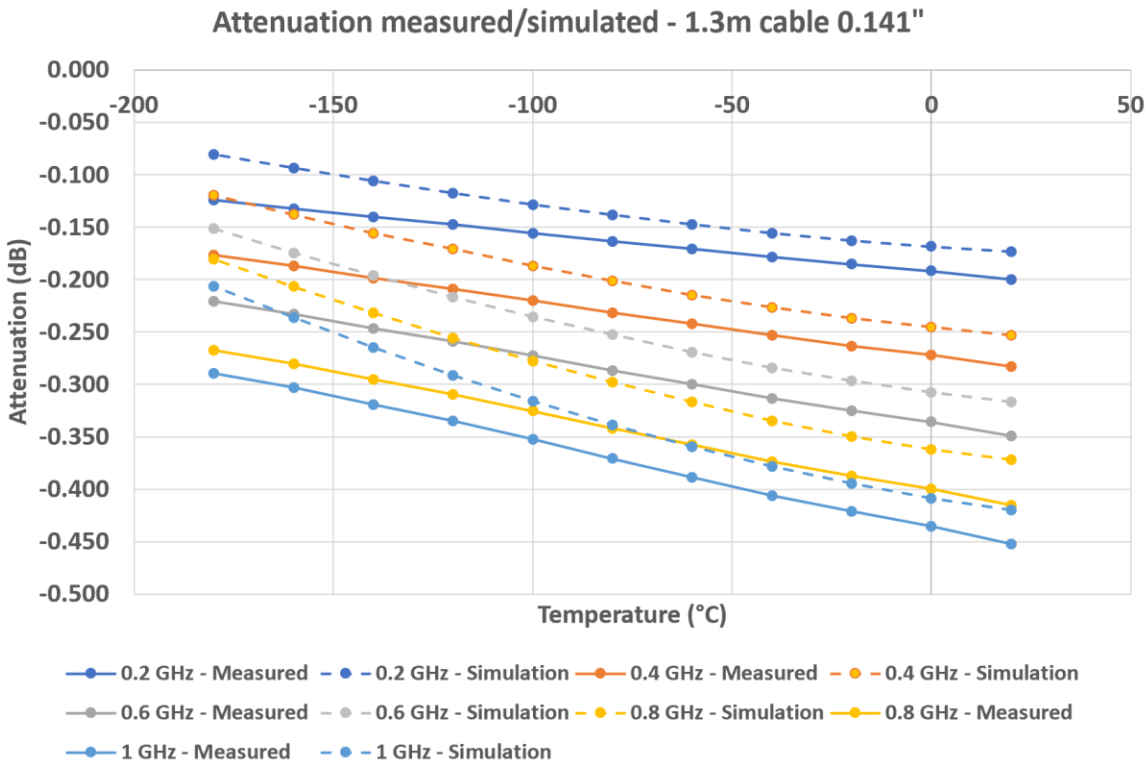


Figure 22 Attenuation measured vs. simulation for a 1.3m long 0.141" cable

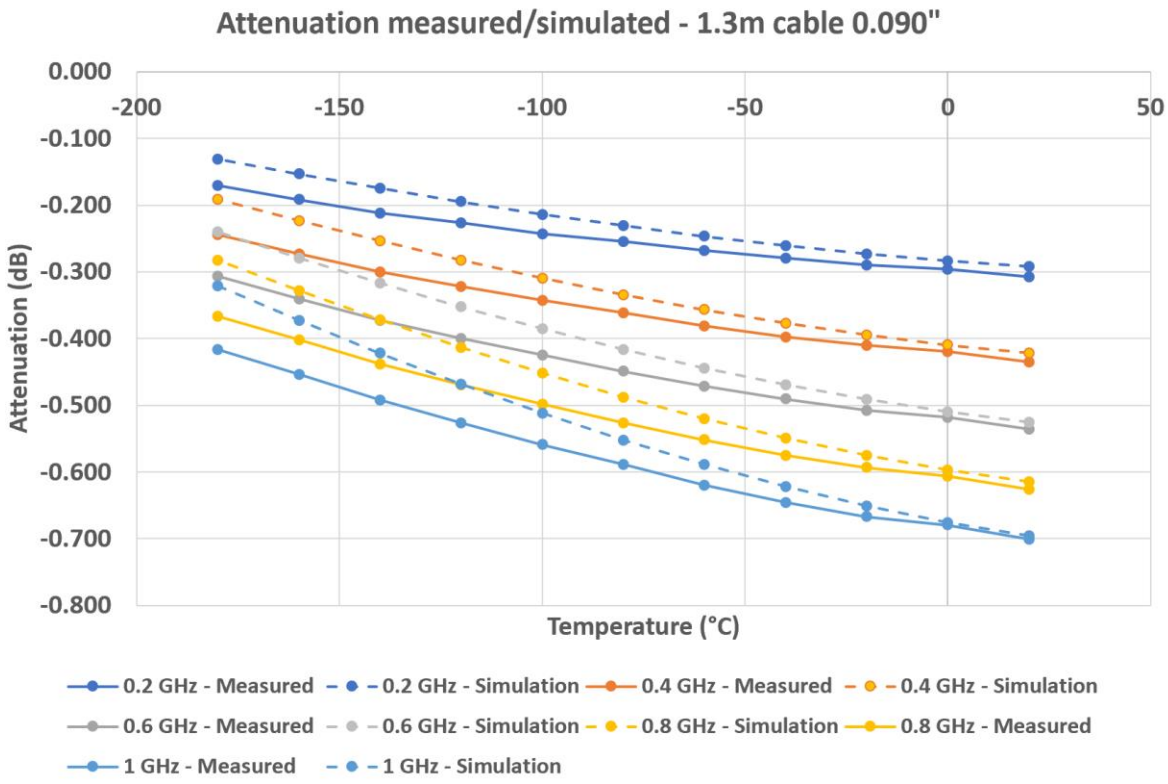


Figure 23 Attenuation measured vs. simulation for a 1.3m long 0.090" cable

Fig. 23 and Fig. 24 depict the attenuation value measured by the manufacturer in solid line versus the simulation with the 1D model in dotted line. Fig.23 corresponds to a 0.141" cable while Fig.24 refers to a 0.090" cable.

For the 0.141" cable (Fig. 1) at 20°C the data are consistent with a maximum difference of 0.050 dB for the high frequency. For the 0.090" cable the data at 20°C are very consistent.

At cold, both in for the 0.141" and 0.090" cables, the measured attenuation is higher than the simulated attenuation. This difference is even higher when the RF frequency is high.

Since the dielectric attenuation is $\propto f$ while the resistive attenuation is $\propto \sqrt{f}$ the fact that the difference is higher at higher frequency points to a dielectric attenuation higher than expected by the model. Another possible explanation would be that the ends of the 5 feet cable was used to transition from room temperature to cryogenic temperature and so was hotter than simulated. Since we simulate an homogeneous temperature along a 5' cable this can explain the attenuation divergence with the experiment at lower temperature.

The difference between the measurement and the simulation can reach 30% at 100 K. However, since most of the attenuation is going to be in the warm section of the cable, the overall impact of this divergence on the BPM model behavior is expected to be limited.

a. Power dissipation

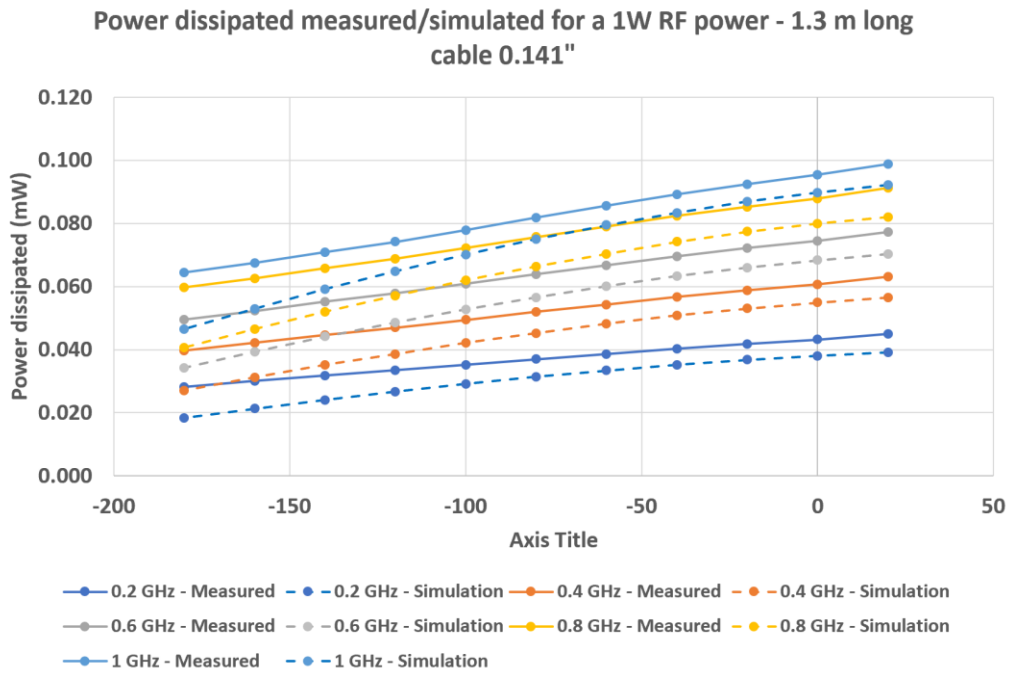


Figure 24 Power dissipation measured vs. simulation for a 1.3m long 0.141" cable

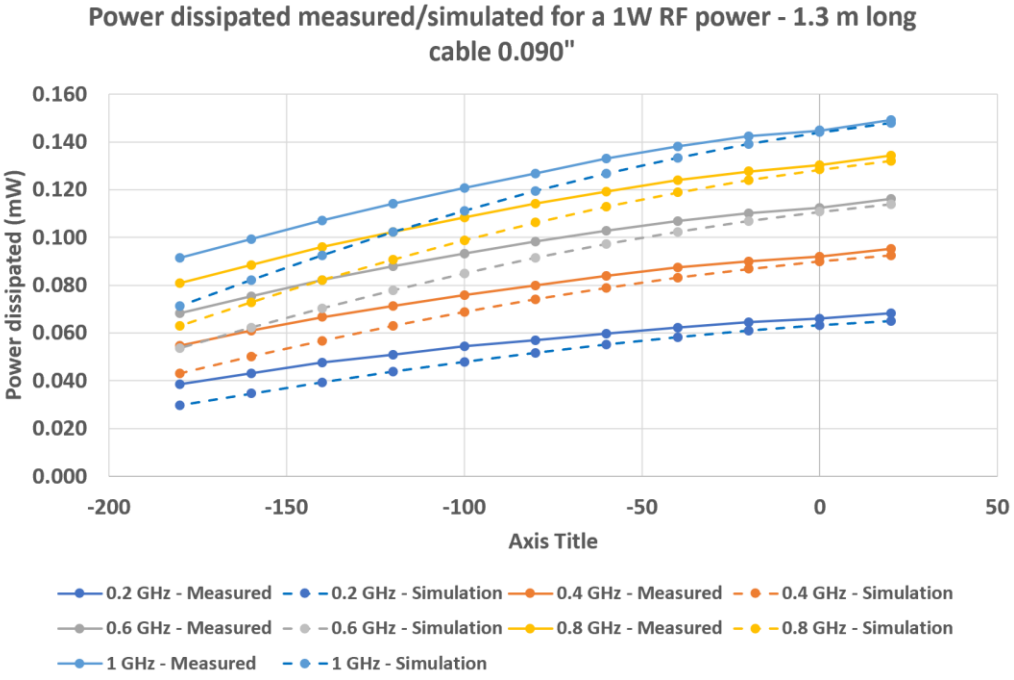


Figure 25 Power dissipation measured vs. simulation for a 1.3m long 0.090" cable.

While the power dissipation data are very consistent at room temperature, their differ at cold temperature like the cable attenuation. The observation and proposed explanation is similar than with the attenuation graphs. Note that a 20% overestimation was done when selecting a reference frequency, this should cover some of this underestimation at lower temperature (while still being conservative at higher temperatures).

Appendix V – Thermal conduction and placement of the heat shield thermalization

Introduction

The RF coaxial cable planned to be used for EIC will produce significantly more heat conduction that the cable used for RHIC mostly because of the material used.

We will aim at describing the initial heat conduction analysis leading to the study of thermalization placement in this section.

Heat conduction

Material and dimensions

Material (ID/OD)	**RHIC**	**EIC – 0.141" cable**	**EIC – 0.090" cable**
Outer conductor	**304L** (ID 3.58mm/OD 3.57mm)	**304L** (ID 3.58mm/OD 3.57mm)	**304L** (ID 1.78mm/OD 2.29mm)
Outer conductor plating	/	**Cu RRR10** (Thickness 0.076mm)	**Cu RRR10** (Thickness 0.076mm)
Dielectric	**Tefzel** (ID 3.07mm/OD 0.81mm)	**Si02** (ID 3.07 mm/OD 1.09 mm)	**Si02** (ID 1.78 mm/OD 0.64 mm)
Inner conductor	**Cu RRR300** (OD 0.81mm)	**Cu RRR300** (OD 1.09mm)	**Cu RRR300** (OD 0.64.mm)

1D thermal conduction comparison

Using the materials and dimensions above, we worked out the linear thermal conduction along the cable in mW.m. We can get an estimated conduction power in multiplying by the actual cable length.

The cable is divided in two stages:

The "hot" stage links the tunnel feedthrough (300K hot sink) to the thermalization piece cooled to the heat shield temperature. The heat shield helium will vary between 50K and 80K depending on the magnet position along the circuit.

The "cold" stage links the thermalization piece (50K to 80K) to the BPM module (considered at 4K).

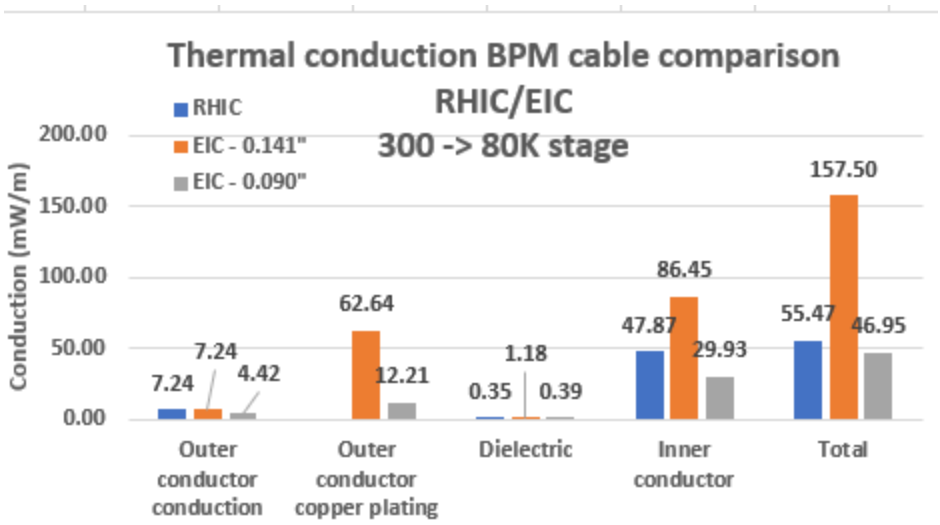


Figure 26 Linear thermal conduction for the hot stage (300K -> 80K) stage for different cables

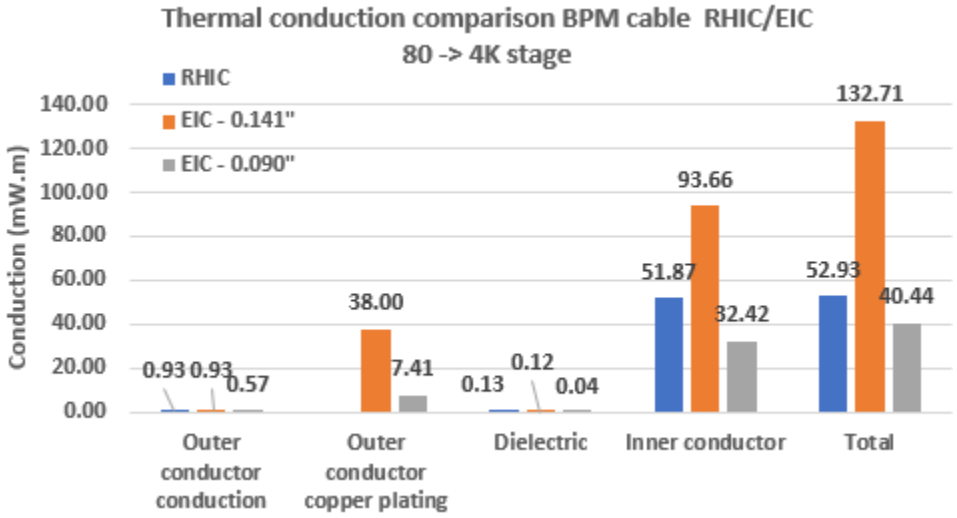


Figure 27 Linear thermal conduction for the cold stage (80K->4K) stage for different cables

From Fig. 1 and Fig. 2 we see that overall, the 0.090" EIC cable will conduct slightly less heat to the cryogenic circuits than the RHIC cable did. The EIC 0.141" cable, however, conducts about 2.5x times more heat to the cryogenic circuit as the RHIC cable for an identical implementation.

Placing the thermalization for EIC

As depicted on Fig. 1 and Fig. 2 the heat flow can be evaluated at the different heat station as a function of the length between these heat stations. We can then work out the placement the heat shield heat station along the cable length to minimize the overall load at the cryoplant.

The length of the cable is considered fixed at 1.3 m. Fig. 3 and Fig. 4 depict the effective heat load at the cold point in function of the distance between the thermalization and the tunnel feedthrough.

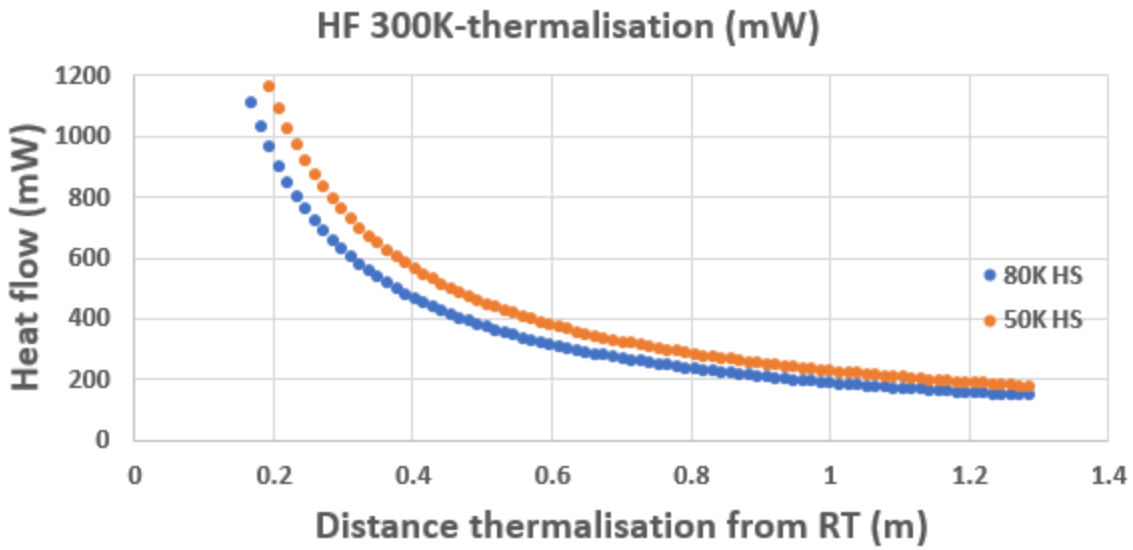


Figure 28 Heat conduction to the heat shield for the EIC 0.141" cable for two heat shield temperature (80K or 50K)

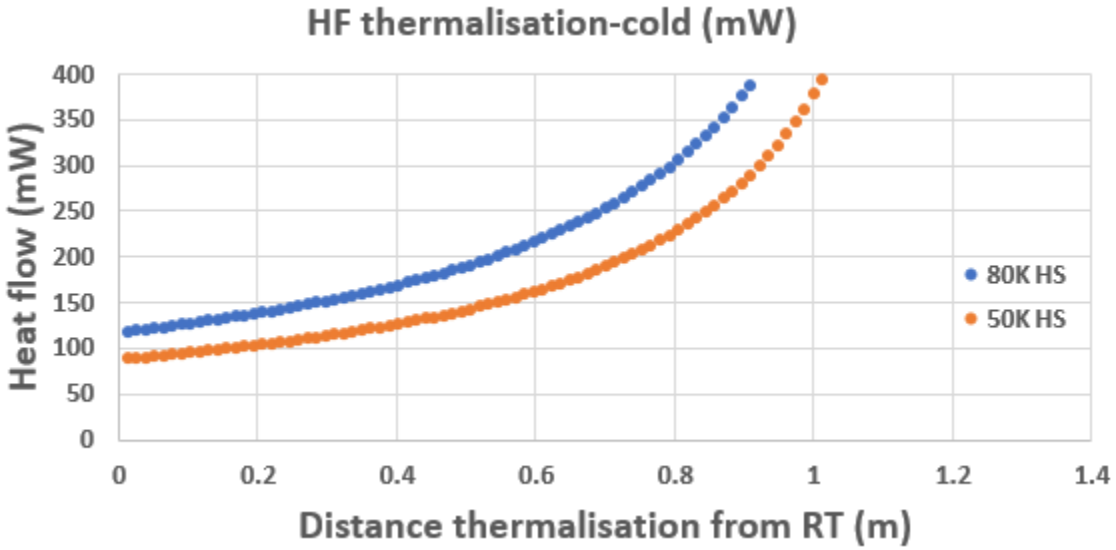


Figure 29 Heat conduction to the 4.5K cooling circuit for the EIC 0.141" cable for two heat shield temperature (80K or 50K)

We will try to place the thermalization to minimize the cryoplant working load. The cryoplant is assumed to follow a Carnot thermodynamic cycle with a 20% efficiency (Ref. [5]). Fig 32 depicts the cryoplant power to extract 1W of heat at different cold temperatures.

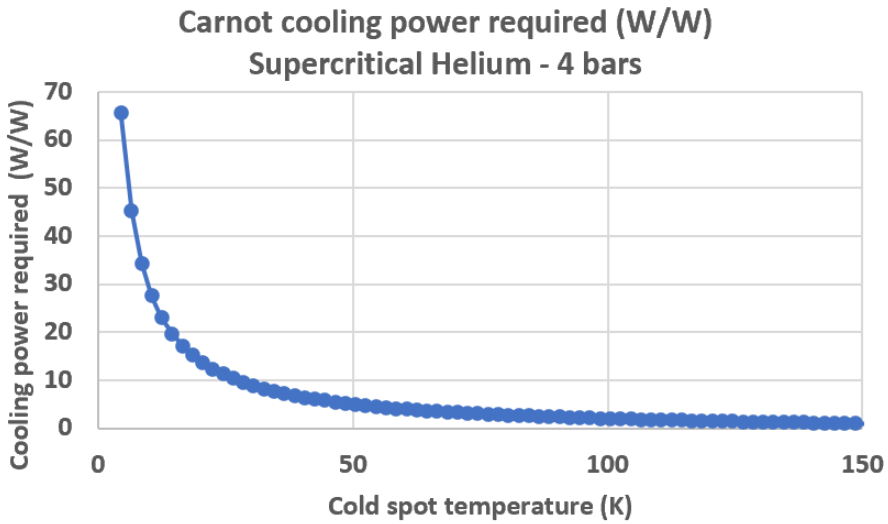


Figure 30 Cryoplant (20% Carnot) power to extract 1W at cold

Using this and the heat flow as a function of the thermalization position (Fig. 30 and Fig. 31) we can work out the power required at the cryoplant as a function of the thermalization placement. Shifting the thermalization toward the hot sink (tunnel feedthrough) will decrease the heat load to the BPM module (4.5K) but increase the heat load on the heat shield (80K/50K). We will strive the place the thermalization where the cryoplant cooling load (= operating cost) is minimized.

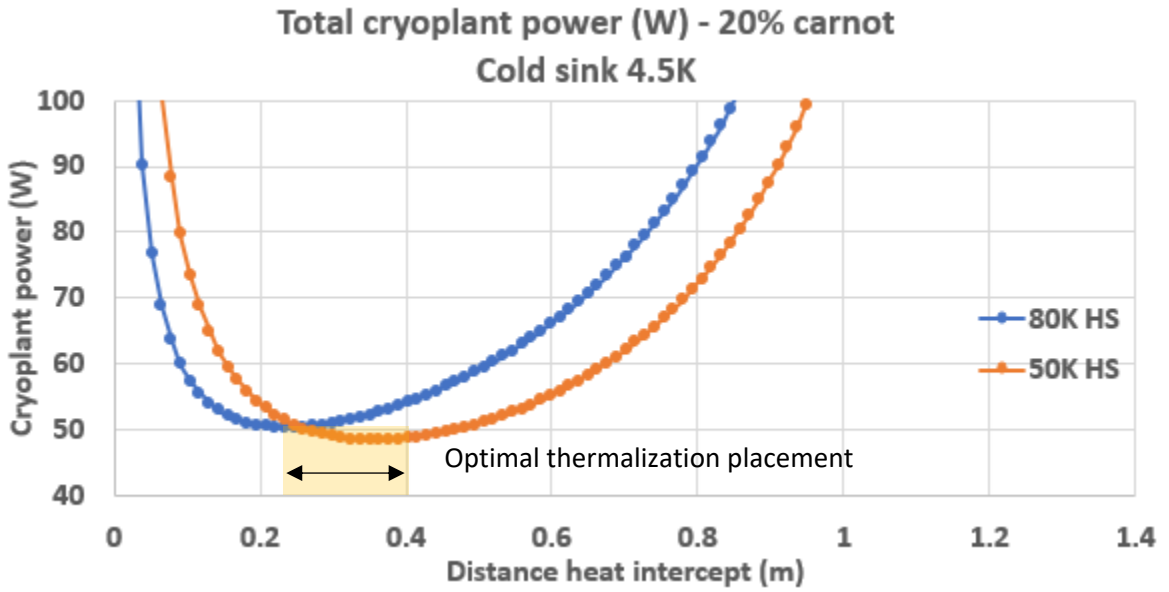


Figure 31 Optimum placement of the thermalisation to minimize the cryoplant working load

As seen on Fig. 33 we should ideally place the thermalization between 0.25 and 0.4 m from the tunnel feedthrough to minimize the operating costs.

Appendix VI - Measuring the HSR BPM cable thermal conduction

F. Micolon, R. Anderson, S. Seberg – September 2023

Version	Date	Modification
0.1	9/14/23	Initial draft

1. Introduction

A significant part of the heat flux brought by the BPM system to the HSR cryogenic circuit is through the coaxial signal cables owing to their copper content. To verify their actual heat conduction a test was carried out in liquid nitrogen.

2. Test principle

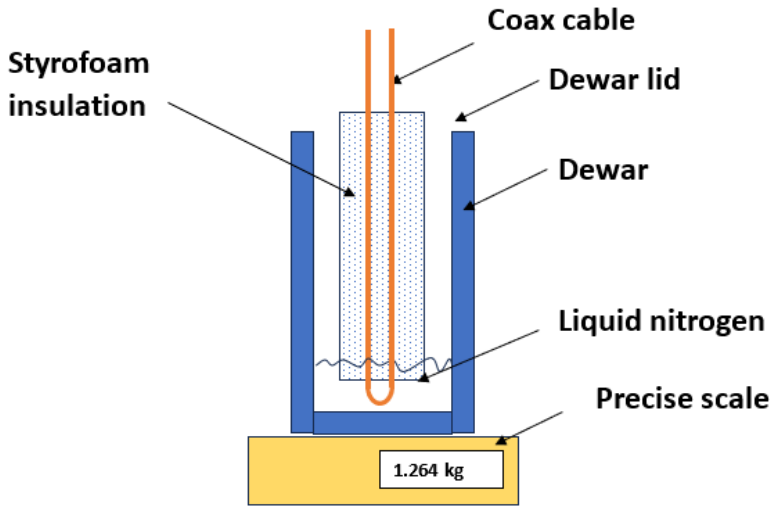


Figure 32 Sketch of principle of the LN2 boil off test

A known length of BPM cable was dipped in liquid nitrogen (LN2) at 77 K. The effective LN2 boil off with and without the cable were compared. This comparison allows us to work out the additional heat from the cable conduction.

Two cables were tested, a folded 0.090” cable with an insulated stretch of 5.5” and a folded 0.141” cable with an insulated stretch of 6.25” (Fig 1).

3. Test results

We can deduce the conducted power from the liquid nitrogen latent heat of evaporation, taken as 199.2 J/g at 1 atm pressure (see table 1).

Table 6 Conducted heat flux in the LN2 bath

Configuration	LN2 additional boil off (g/h)	Conducted power (W)
Baseline (dewar only)	0	0
2x 0.090” cable 5.5” long	-10.5	0.581
2x 0.141” cable 6.25” long	-25.2	1.394

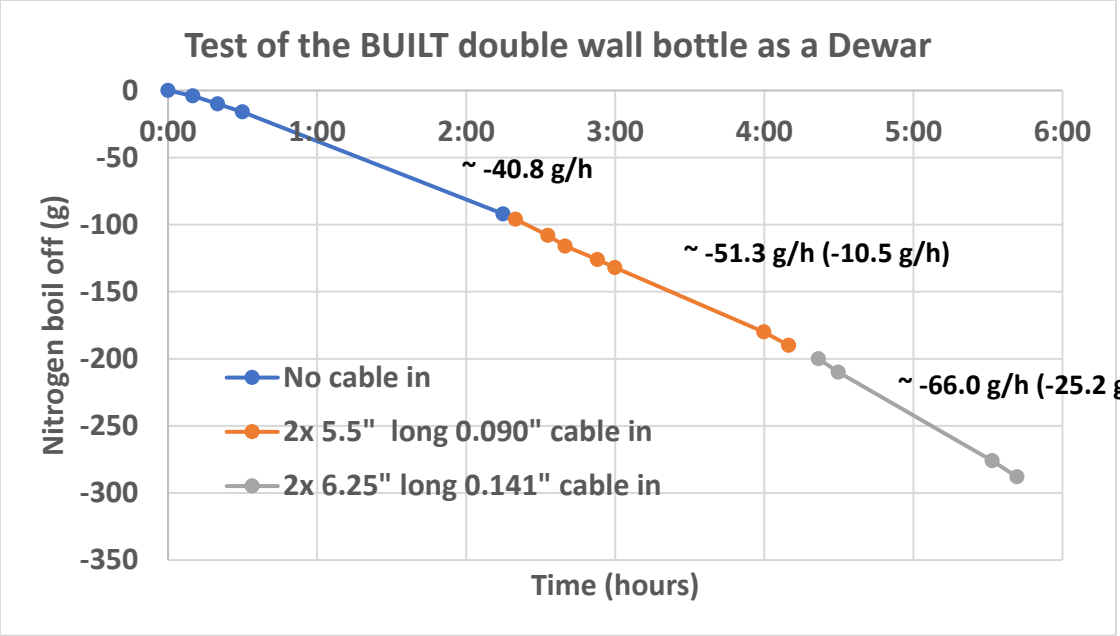


Figure 33 LN2 boil off test results. Boil off value are next to the curve.

4. Comparison with analytical data and discussion

Working out the thermal conductivity integral from 273 K to 80 K for the respective cable composition, we expect that a 0.141" cable should conduct 139.4 mW/m and a 0.090" cable 41.6 mW/m.

Table 2 displays the experimental vs analytical heat conduction.

Table 7 Comparison analytical vs measured conduction.

Configuration	Analytical conduction (mW)	Measured conduction (mW)	Difference
2x 0.090" cable 5.5" long	596	581	-3 %
2x 0.141" cable 6.25" long	1756	1394	-25 %

The 0.090" conduction matches closely with the expectations but the 0.141" cable has a conduction 25% lower than anticipated (table 2). The 0.141" cable inner conductor diameter was measured slightly smaller than nominal (0.0415" vs 0.043"), it is probable that the copper coating thickness on the outer conductor is on the lower bound of its tolerance (0.003" +/-0.0015"). With the smaller inner conductor diameter (0.0415") and the thinnest copper coating (0.0015") the expected analytical conduction would be 1346 mW which matches the experiment result (1394 mW).

Note: An important caveat of this test to predict the cable conduction to 4 K is that the RRR of copper is unknown. RRR values will strongly affect the thermal conductivity of copper between 80 K to 4 K. Above 80 K the copper conductivity is practically RRR-unsensitive. Thanks to that, this test gives a reliable feedback on the actual copper content of the cable design (since conductivity is not also coupled to copper RRR). However, a negative side effect is that the actual heat conducted at 4 K cannot be reliably inferred from this test alone.

Conclusion

A simple experiment has been carried out to validate the cable heat conduction to liquid nitrogen. While the conduction value measured matches our expectations for the 0.090” cable, it is lower than expected for the 0.141” cable. This is thought to be due to copper conductor dimensions on the lower end of the tolerance range.

Appendix VII – Heat shield thermal resistance

Introduction

The heat shield intercept is attached to the heat shield with aluminum braids (see Fig 1). The braid and the heat shield itself represent a significant thermal resistance to the BPM cable heat extraction. Evaluating this thermal resistance is important to get a correct modelling of the cable temperature profile.

Aluminum braid thermal resistance

Based on drawing 81015098 we find that the aluminum braid has a length of 6” between bolting holes (measured on an existing magnet), a thickness of 0.06” and a width of 1”. Assuming a filling factor of 50%, but with two parallel braids installed. We can the work out its thermal resistance:

$$\frac{\Delta T}{P} = \frac{L}{k.A} = \frac{6.25{,}4E-3}{320.((0{,}06.25{,}4E-3).(1.25{,}4E-3).0{,}5.2} = 12{,}3\ K/W$$

Heat shield thermal resistance

A model of the heat shield was made to work out its thermal resistance (see Fig. 35) :

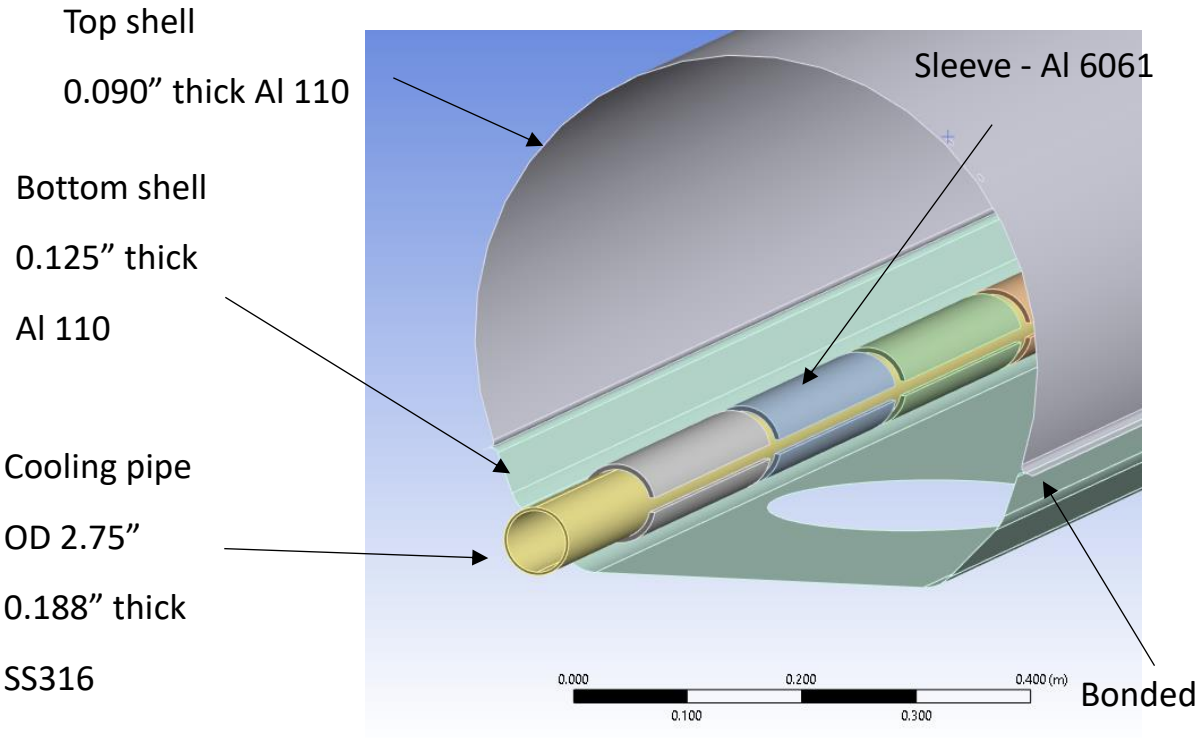


Figure 34 Heat shield model

The boundary conditions are detailed in Fig 36 :

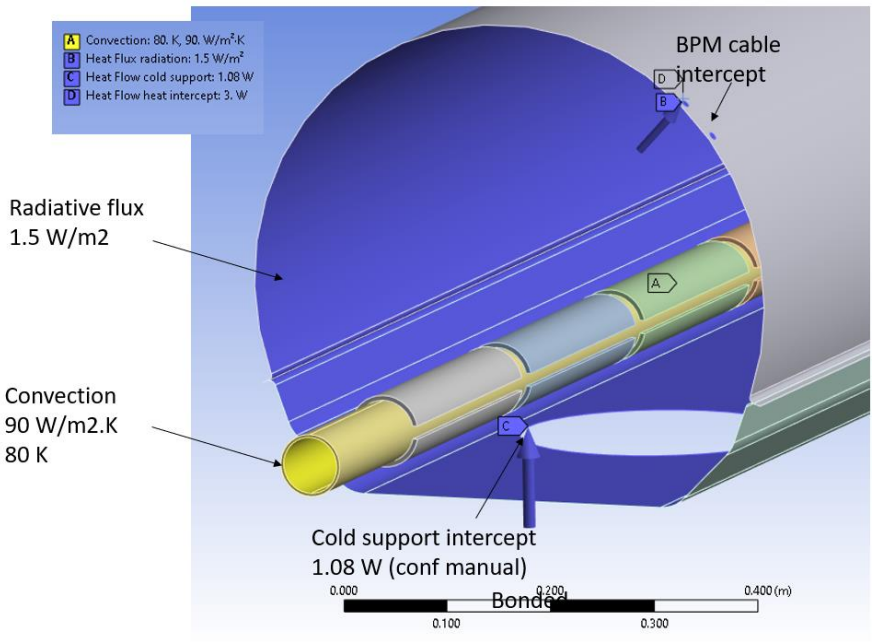


Figure 35 Heat shield model boundary conditions

The results plot shows the resulting shield to braid hole temperature versus heat flux brought in by the braid.

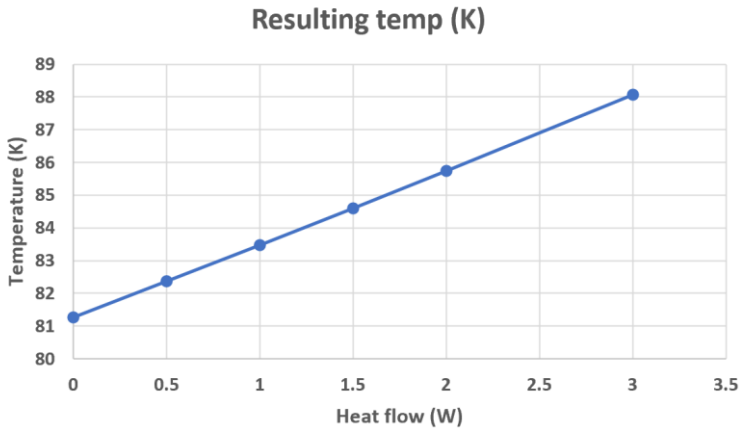


Figure 36 Heat shield interface temperature versus heating power

The slope of the curve depicted in Fig. 37 shows an additional 2.3 K/W of thermal resistance. The overall thermal resistance, braid and heat shield is then (12.3+2.3) = 14.3 K/W. This can be distributed on all four cables interfaces.